FORESTRY AND NATURAL SCIENCES

ANTTI NISSINEN

Modelling Errors in Electrical Impedance Tomography

UNIVERSITY OF
EASTERN FINLAND

ANTTI NISSINEN

Modelling errors in electrical impedance tomography

Academic Dissertation
To be presented by permission of the Faculty on Natural Sciences and Forestry
for public examination in the Auditorium L22 in Snellmania Building at the
University of Eastern Finland, Kuopio, on June, 3, 2011,
at 12 o'clock noon.

Department of Applied Physics

Author's address: University of Eastern Finland
                     Department of Applied Physics
                     P.O.Box 1627
                     70211 KUOPIO
                     FINLAND
                     email: antti.nissinen@uef.fi

Supervisors: Professor Jari Kaipio, Ph.D.
                     University of Auckland
                     Department of Mathematics
                     Private Bag 92019, Auckland Mail Centre
                     1142 AUCKLAND
                     NEW ZEALAND
                     email: jari@math.auckland.ac.nz

                     Docent Ville Kolehmainen, Ph.D.
                     University of Eastern Finland
                     Department of Applied Physics
                     P.O.Box 1627
                     70211 KUOPIO
                     FINLAND
                     email: ville.kolehmainen@uef.fi

Reviewers: Professor Simon Arridge, Ph.D.
                     University College London
                     Department of Computer Science
                     WC1E 6BT
                     LONDON
                     UK
                     email: Simon.Arridge@cs.ucl.ac.uk

                     Professor Helcio Orlande, Ph.D.
                     Federal University of Rio de Janeiro
                     Department of Mechanical Engineering
                     RJ, 21941-972
                     RIO DE JANEIRO
                     BRAZIL
                     email: helcio@mecanica.ufrj.br

Opponent: Professor Samuli Siltanen, Ph.D.
                     University of Helsinki
                     Department of Mathematics and Statistics
                     P.O. Box 68 (Gustaf Hällströmin katu 2b)
                     FI-00014 HELSINKI
                     FINLAND

ABSTRACT

In electrical impedance tomography (EIT), electrodes are attached on the boundary of the object and currents are injected into the object. The voltages are measured using the same electrodes and the conductivity of the object is reconstructed based on the measured voltages. The reconstruction problem is a non-linear ill-posed inverse problem, i.e. the problem is highly sensitive to measurement and approximation errors. The effect of the measurement errors can be reduced by using an accurate measurement system and by accurate modeling of the statistics of the error.

Approximation errors are due to an approximative computational model used in the inverse computations. In practical applications, an adequately accurate mathematical model cannot often be used due to limited computational resources, and therefore a reduced model has to be used. Furthermore, in some cases the accurate model is not available due to unknown shape of the body or unknown nuisance parameters in the computation model, for example. These approximation errors can cause severe reconstruction errors with conventional measurement error models.

Recently, the approximation error approach was proposed for the treatment of the approximation errors. The key idea in the approximation error approach is to represent the approximation errors as a noise process in the measurement model. The statistical model of the approximation error is constructed and then this model is used in the inverse problem to compensate for the approximation errors.

In this thesis, the approximation error approach is applied for several approximation errors in EIT. The approximation errors that are considered are due to reduced discretization, unknown contact impedances, domain truncation and unknown shape of the body. Furthermore, the approximation error approach is employed in a novel way enabling estimation of the conductivity and the shape of the body. All test cases are evaluated by using simulated and real data. The results indicate that the effect of these errors can be efficiently compensated for by the approximation error approach.

Acknowledgments

This study was carried out in the Department of Applied Physics at the University of Eastern Finland (previously University of Kuopio) during the years 2006-2010.

I am grateful to my principal supervisor Professor Jari Kaipio, PhD., for his ideas and guidance during this work. I also thank him for the opportunity to work in this exciting research field in the inverse problems research group. I am also grateful to my supervisor Docent Ville Kolehmainen, PhD., for his guidance in research work. Particularly, his advises in scientific writing has been invaluable for me.

I wish to thank the official pre-examiners Professor Simon Arridge, PhD., and Professor Helcio Orlande, PhD., for the assessment of the thesis.

I would like to thank the staff of the Department of Applied Physics for their support. Especially, I thank my co-author Lasse Heikkinen, PhD., for excellent advises and help during these years. I would like to thank Tuomo Savolainen, PhD., and Jari Kourunen, M.Sc., for assistance with EIT laboratory measurements. I thank all my colleagues in the inverse problem group for the support and for the pleasant working atmosphere. Especially, I thank Kimmo Karhunen, M.Sc., and Ville Rimpilinen, M.Sc. (Tech.), for their friendship. I thank my former roommates Simo-Pekka Simonaho, PhD., Antti Lipponen, M.Sc. and Gerardo del Muro Gonzalez , M.Sc, for their support and for academic and non-academic discussions.

I want to express my gratitude to my mother Eeva and to my sister Anna and brothers Pertti and Arto. I also thank all my relatives and friends for the support and friendship during these years.

Kuopio March 30, 2011   *Antti Nissinen*

ABBREVIATIONS

AEM   Approximation error model
2D   Two-dimensional
3D   Three-dimensional
CEM   Conventional error model
CM   Conditional mean
CT   Computerized tomography
EIT   Electrical impedance tomography
FEM   Finite element method
GN   Gauss-Newton
LS   Least squares
MAP   Maximum a posteriori
MCMC   Markov chain Monte Carlo
MRI   Magnetic resonance imaging

NOTATIONS

$(\cdot)_*$	Expectation value
$(\cdot)^{(\ell)}$	ℓth sample
$(\tilde{\cdot})$	Approximative model
$\pi(\cdot)$	Probability density
$A(x)$	Forward model
$A_h(x)$	FEM approximation of forward model
α	Regularization parameter, projection coefficient vector
d	Nuisance parameter
e	Measurement noise
e_ℓ	ℓth electrode
ε	Approximation error
ε'	Low-rank projection of ε
η	Sum of measurement and modelling errors
γ	Parameterization of $\partial\Omega$
Γ	Covariance matrix
h, δ	Discretization level parameter
m	Number of measurements
N	Dimension of conductivity vector
n	Outward unit normal vector
N_s	Number of samples
N_e	Number of elements
N_n	Number of nodes
N_{el}	Number of electrodes
Ω	Computation domain
$\partial\Omega$	Boundary of domain
σ	Conductivity
x	Parameter vector, position vector
y	Measurement vector
u	Potential distribution
U	Electrode potential
V	Measured electrode voltage
z	Contact impedance

LIST OF PUBLICATIONS

This thesis consists of an overview and the following four original articles which are referred to in the text by their Roman numerals I-IV:

I A. Nissinen, L. M. Heikkinen, and J. P. Kaipio, "The Bayesian approximation error approach for electrical impedance tomography—experimental results," *Meas. Sci. Technol.* **19,** 015501 (2008).

II A. Nissinen, L. M. Heikkinen, V. Kolehmainen, and J. P. Kaipio, "Compensation of errors due to discretization, domain truncation and unknown contact impedances in electrical impedance tomography," *Meas. Sci. Technol.* **20,** 105504 (2009).

III A. Nissinen, V. Kolehmainen, and J. P. Kaipio, "Compensation of modelling errors due to unknown domain boundary in electrical impedance tomography," *IEEE Trans. Med. Im.* **30(2),** 231-242 (2011).

IV A. Nissinen, V. Kolehmainen, and J. P. Kaipio, "Reconstruction of domain boundary and conductivity in electrical impedance tomography using the approximation error approach," *International Journal for Uncertainty Quantification* **accepted,** (2011).

The original articles have been reproduced with permission of the copyright holders.

AUTHOR'S CONTRIBUTION

All publications are result of joint work with the supervisors and co-authors. The author wrote Publications I-III in co-operation with supervisors and also participated for the writing process of Publication IV. The author implemented all the numerical computations using Matlab® and computed all the results in Publications I-IV. Some of the EIT codes such as finite element solvers have been previously developed in the inverse problems group in the Department of Applied Physics. The author conducted the measurements in collaboration with Dr. Lasse Heikkinen.

Contents

1 Introduction

In electrical impedance tomography (EIT), electrodes are attached on the boundary of an object and currents are injected into the object through these electrodes. The voltages on all electrodes are measured and the conductivity of the object is reconstructed based on the measured voltages and known currents; for reviews on EIT, see [1–5].

Electrical impedance tomography has numerous applications in biomedicine, industry, geology and nondestructive testing. The biomedical applications include the monitoring of the lungs and heart [1, 6–9], breast cancer detection [10, 11], and imaging of human brain activity [12]. Examples of the industrial applications include the imaging of the multi-phase flows [13–16], the behavior of the air-core within the hydrocyclone [17], sensor for optimal control [18], slurry mixing [19], and separation [20]. The geophysical applications include leak detection of waste storage tanks [21], hydraulic barrier monitoring [22], and soil water content variations [23]. The nondestructive testing applications include the imaging of concrete [24], for example.

The reconstruction of the conductivity is a non-linear, ill-posed inverse problem, which is highly sensitive to measurement and approximation errors. The effect of the measurement errors can be reduced by using an accurate measurement system and by careful modeling of the statistics of the measurement error, see for example [25].

The approximation errors, on the other hand, are related to discretization of the forward model and approximations in the forward model. In several applications, the forward model has to be reduced since the computation resources and time are limited. The forward model can be reduced using, for example, coarser discretization or reducing the size of the computational domain. Further, one has to use an approximative model when the forward model con-

tains inaccurately known nuisance parameters. For example, the parameterization of the boundary of the body can be unknown in biomedical applications of EIT. One such application is EIT chest imaging in which the accurate shape of the chest is unknown and the shape is time dependent due to breathing. Another typical example of unknown nuisance parameters are the electrode contact impedances. Most of the current approaches to EIT treat the contact impedances as known, fixed parameters. However, in practical measurements they are always unknown and can change during the measurements. For example, in industrial applications the contamination of the surface of the electrodes can change the contact impedances locally and temporally as well.

The reconstruction errors due to approximation errors can be reduced by using the recently proposed Bayesian approximation error approach [26,27]. The key idea in the approximation error approach is, loosely speaking, to represent not only the measurement error, but also the effects of the computational model errors and uncertainties as an auxiliary additive noise process in the observation model. The realization of the approximation error is obviously unknown since its value depends on the actual unknown conductivity and possibly on uncertainly known nuisance parameters in the forward model. However, the statistics of the related approximation error can be estimated over the prior distribution models. The statistical model of the approximation error is then used in the reconstruction process to compensate for the effect of the approximation errors.

The approximation error approach was originally applied for model reduction errors in EIT with numerical examples in [26]. After that the approximation error approach has been applied for different approximation errors and also for other inverse problems. The approximation error approach for the marginalization of unknown nuisance parameters was proposed in [28]. The computed examples were related to optical tomography in which the absorption coefficient is usually the primarily interesting parameter and the scattering coefficient can be considered as a nuisance parameter.

In geophysical EIT, the discretization errors and errors due to truncation of the computational domain were studied in [29]. In [30], linear approximation for the forward solution was used in EIT inverse problem and the linearization error was treated by using the approximation error approach. In optical tomography, model reduction, domain truncation and unknown anisotropy structures were treated in [31–34]. In [35], again related to optical tomography, an approximative physical model (diffusion model instead of the radiative transfer model) was used for the forward problem.

The aim of this thesis is to apply the approximation error approach to approximation errors in EIT. The approximation errors that are considered are the errors due to reduced discretization, truncation of the computation domain, unknown electrode contact impedances, and unknown shape of the body. The approximation error approach is evaluated with real laboratory measurements in all cases. These approximation errors are pivotal in EIT, since they make the computation of the feasible reconstructions excessively time consuming or impossible when the conventional measurement error models are employed.

In this thesis, following case studies of the approximation error approach are considered:

1. The first study concern a process monitoring application. The studied approximation errors are due to reduced discretization and partially unknown geometry of the target. The geometry of the target is partially unknown due to unknown height of the liquid in the laboratory vessel. By employing the approximation error approach feasible reconstructions can be computed using reduced discretization and by using approximative computation domain.

2. The approximation error approach is applied for errors due to discretization, truncation of the computation domain and unknown contact impedances. These approximation errors are encountered in a flow monitoring application. By using the approximation error approach, the computation time can be

reduced significantly. Furthermore, the solution of the inverse problem becomes less complicated since the electrode contact impedances does not have to be estimated.

3. The approximation errors due to reduced discretization and unknown shape of the body are reduced by employing the approximation error approach. The computed examples concern the chest imaging problem in which the shape of the chest is unknown. The cross-section of the chest is modeled with a model domain which is used in the inverse problem. The approach is evaluated both with simulated measurements and measurements from a chest phantom.

4. The reconstruction of the conductivity and the shape of the body is proposed. The approximation error approach is employed in a novel way enabling the simultaneous estimation of the conductivity and a low rank approximation for the unknown realization of the approximation error. In the second stage of the approach, the unknown shape of the body is estimated based on the approximative joint distribution of the approximation error and the parameterization of the boundary shape. The computed examples concern the EIT chest imaging application.

This thesis is organized as follows. The Bayesian framework for the inverse problems and the approximation error approach is reviewed briefly in Chapter 2. Furthermore, the previous applications of the approximation error approach are also reviewed in Chapter 2. In Chapter 3, the forward model and notations in the EIT forward model are represented. The reconstruction problem in EIT is also reviewed in Chapter 3. The review of the results is given in Chapter 4. In Chapter 5, summary and conclusions of the thesis are given.

2 Inverse problem in statistical framework

In this chapter, we present a brief review on inverse problems in the statistical framework and typical estimates computed using this approach. Furthermore, a review on approximation error approach is also given. For more details of the Bayesian framework for inverse problems in general see [2, 26, 36, 37] and for approximation error approach, see [26–28, 31].

We consider the inverse problem of estimating x given indirect noisy observations (measurements) y. The model that relates the measurements y and quantity x is $y = A(x, d) + e$, where $A(x, d)$ is the forward operator, d is a vector of possibly unknown nuisance parameters and e is the measurement noise.

2.1 INVERSE PROBLEM

2.1.1 Construction of the posterior model

The discussion is mainly based on the references [26, 28, 31]. In the Bayesian framework, all unknowns and measurements are considered as random variables and the uncertainty related to their values is encoded in their probability distribution models. The joint probability density of the parameter x, nuisance parameter d, and measurements y can be written as

$$\pi(x, d, y) = \pi(x, d)\pi(y \mid x, d) = \pi(y)\pi(x, d \mid y), \qquad (2.1)$$

where $\pi(y \mid x, d)$ is the *likelihood model* and the probability density $\pi(x, d)$ is the *prior model* of x and d. The posterior density, which is given by the Bayes formula

$$\pi(x, d \mid y) = \frac{\pi(y \mid x, d)\pi(x, d)}{\pi(y)}, \qquad (2.2)$$

is the complete probabilistic model of the inverse problem and represents the uncertainty in the unknowns given the measurements.

In conventional approaches to inverse problems, the nuisance parameter d is assumed to be known. Let $\tilde{d}$ denote a fixed value for the parameter d. In the sequel, the tilde $\tilde{}$ refers to the models that are to be used in the inversion. In the Bayesian formulation, all variables that are known, such as measurements, or *are treated as* fixed parameters, appear as conditioning variables. Thus, if we fix $d = \tilde{d}$, instead of $\pi(x, d \mid y)$ in (2.2), we actually consider

$$\pi(x \mid y, d = \tilde{d}) = \frac{\pi(y \mid x, d = \tilde{d})\pi(x)}{\pi(y)}. \tag{2.3}$$

Formally, the uncertainty in the primary interesting unknown x is obtained by marginalization (integrating) over d in (2.2)

$$\pi(x \mid y) = \int \pi(x, d \mid y) \, dd. \tag{2.4}$$

The posterior uncertainty of x that is predicted by (2.3) is usually significantly overoptimistic when compared to the actual uncertainty given by (2.4). In addition, any point estimates, such as the maximum a posteriori estimate, are bound to be highly misleading. It is important to note that $\pi(x \mid y) \neq \pi(x \mid y, d')$ generally with *any d'*.

Unfortunately, the integral in (2.4) does not generally have an analytical solution and can be computed only with the often excessively resource demanding Markov chain Monte Carlo approach, see for example [26, 38–40]. For this reason, approximations are usually needed to be considered in applications with limited computational resources.

2.1.2   Point and spread estimates

In practice, the posterior density is often high dimensional which makes direct interpretation and visualization infeasible. For example, in image reconstruction problems the dimension of the posterior density can be several thousands. To interpret and visualize

the solution, one computes point estimates from the posterior. One of the most commonly used point estimate is the maximum a posteriori (MAP) estimate

$$x_{\text{MAP}} = \arg\max \pi(x \mid y). \qquad (2.5)$$

The computation of the MAP estimate leads to an optimization problem. Another commonly used point estimate is the conditional mean (CM) estimate. The computation of the CM estimate of the posterior density leads to an integration problem

$$x_{\text{CM}} = \int x\pi(x \mid y)\,dx. \qquad (2.6)$$

The integration problem can be solved by using Markov chain Monte Carlo (MCMC) methods.

In statistical framework, the reliability of the point estimates can be assessed by computing spread estimates. The conditional covariance is defined as

$$\text{cov}(x \mid y) = \int (x - x_{\text{CM}})(x - x_{\text{CM}})^{\text{T}}\pi(x \mid y)\,dx. \qquad (2.7)$$

The computation of the conditional covariance is also an integration problem.

2.2 CONVENTIONAL ERROR MODEL

2.2.1 Construction of the posterior model

The measurements are commonly modeled with the Gaussian additive noise model

$$y = A(x,d) + e, \quad e \sim \mathcal{N}(e_*, \Gamma_e) \qquad (2.8)$$

where $A(x,d)$ is a non-linear forward model and e is a Gaussian distributed noise vector with mean e_* and covariance matrix Γ_e. If parameters x, d and e are mutually independent, the likelihood can be written as

$$\pi(y \mid x,d) = \pi_e(y - A(x,d)), \qquad (2.9)$$

where π_e is the probability density of the noise e. Moreover, let the prior model be the Gaussian distribution $\mathcal{N}(x_*, \Gamma_x)$,

$$\pi(x) \propto \exp\left(-\frac{1}{2}(x - x_*)^{\mathrm{T}}\Gamma_x^{-1}(x - x_*)\right)$$

where $x_* \in \mathbb{R}^N$ is the prior mean and Γ_x the prior covariance matrix.

Then, the posterior density of x given *both* the measurements y *and* the parameter d becomes

$$\pi(x \mid y, d) \propto \exp\left(-\frac{1}{2}(x - x_*)^{\mathrm{T}}\Gamma_x^{-1}(x - x_*)\right.$$
$$\left. -\frac{1}{2}(y - A(x, d) - e_*)^{\mathrm{T}}\Gamma_e^{-1}(y - A(x, d) - e_*)\right).$$
$$(2.10)$$

Note that the distribution (2.10) represents the posterior uncertainty in x *only if* the d that is used as a fixed parameter in (2.10), corresponds to the actual value of the parameter.

2.2.2 MAP-estimate with conventional error model

The MAP-estimate of the posterior density (2.10) is computed as follows

$$\begin{aligned}
x_{\mathrm{MAP}} &= \arg\max \pi(x \mid y, d) \\
&= \arg\min \left\{ \|L_e(y - A(x, d) - e_*)\|^2 \right. \\
&\quad + \left. \|L_x(x - x_*)\|^2 \right\},
\end{aligned}$$
$$(2.11)$$

where L_e and L_x are Cholesky factors such that

$$\Gamma_e^{-1} = L_e^{\mathrm{T}}L_e, \quad \Gamma_x^{-1} = L_x^{\mathrm{T}}L_x.$$

The minimization problem (2.11) can be solved, for example, by the Gauss-Newton algorithm [41]. We refer to (2.11) as *MAP with conventional error model* (MAP-CEM).

2.3 APPROXIMATION ERROR APPROACH

In this section, the approximation error approach is formulated to account for discretization errors and errors due to unknown parameters d in the forward model $A(x,d)$. Typically, the solution of the forward model is computed using some numerical method such as finite element method FEM [42]. In this section, the FEM solution of the forward model $A(x,d)$ is denoted as $A_h(x,d)$ where h is the discretization level parameter controlling the mesh density and $x \in \mathbb{R}^{N_n}$. It follows from the theory of finite element method that [42]

$$A_h(x,d) \to A(x,d) \text{ as } h \to 0 \quad \text{and } N_n \to \infty$$

Let

$$y = A_\delta(\bar{x},d) + e, \tag{2.12}$$

denote a (sufficiently) *accurate model* between the unknowns and measurements. Here the parameter d and discretization level parameter δ are such that the error in the FEM approximation is smaller than the measurement error. The parameterization $\bar{x}$ is dense enough in the above sense.

In practical applications, the nuisance parameter d is often unknown. Furthermore, for reasons related to the computation time and resources, there is often pressure to keep the discretization level of the forward model relatively coarse. In such a case, the accurate model (2.12) is replaced by the approximate measurement model:

$$y \approx A_h(x,\tilde{d}) + e, \tag{2.13}$$

where the discretization level parameter $h > \delta$ and $\tilde{d}$ is the approximative nuisance parameter vector, and one hopes that the approximation in (2.13) is a feasible one. The relation of the representation of the parameters x and $\bar{x}$ in (2.12) and (2.13) is of the form

$$P\bar{x} = x, \tag{2.14}$$

where P is a matrix that interpolates the parameter $\bar{x}$ in the model (2.12) to parameter x in the model (2.13). The model $A_h(x,\tilde{d})$ is the

model that is to be used in the inversion, that is, the discretization level and the parameters $\tilde{d}$ are fixed. We refer to the model $A_h(x,\tilde{d})$ in (2.13) as the *target model*.

2.3.1 Construction of approximative posterior model

In the approximation error approach, instead of writing the approximation (2.13), the *accurate measurement model* (2.12) is written in the form

$$
\begin{aligned}
y &= A_h(x,\tilde{d}) + \left(A_\delta(\bar{x},d) - A_h(x,\tilde{d})\right) + e \\
&= A_h(x,\tilde{d}) + \varepsilon(\bar{x},d) + e \\
&= A_h(x,\tilde{d}) + \eta,
\end{aligned}
\tag{2.15}
$$

where $\varepsilon(\bar{x},d)$ represents the approximation error due to the discretization and approximative parameter $\tilde{d}$, and we denote $\eta = \varepsilon + e$. Being a function of random variables, ε is a random variable and the joint density $\pi(\varepsilon,\bar{x},d)$ as well as the marginal density $\pi(\bar{x},\varepsilon)$ can be computed in principle, but in most cases these do not have analytical expressions.

The objective in the approximation error approach is to derive a computationally efficient approximation $\tilde{\pi}(x \mid y)$ for the posterior density $\pi(x \mid y)$ based on the measurement model (2.15). When x and d are modelled as mutually independent, and the only term that depends on the random variable d in (2.15) is η, the posterior model corresponding to (2.15) can be written as

$$
\tilde{\pi}(x \mid y) = \underbrace{\pi_{\eta|x}(y - A_h(x,\tilde{d}) \mid x)}_{\pi(y|x)}\, \pi(x),
\tag{2.16}
$$

see [28] for details. A complication is that the likelihood $\pi(y \mid x)$ in (2.16) does not in general have an analytic expression. To obtain a computationally feasible and efficient approximation $\tilde{\pi}(x \mid y)$, we make the Gaussian approximation for the joint distribution $\pi(x,\eta)$. This is the core of the most common implementation of the approximation error approach, in particular when computational

efficiency is sought. Then, we obtain the Gaussian approximation for the likelihood in (2.16), and the approximation for the posterior model becomes:

$$\tilde{\pi}(x \mid y) \propto \exp\left(-\frac{1}{2}(x - x_*)^{\mathrm{T}}\Gamma_x^{-1}(x - x_*)\right.$$
$$\left. -\frac{1}{2}(y - A_h(x,\tilde{d}) - \eta_{*|x})^{\mathrm{T}}\Gamma_{\eta|x}^{-1}(y - A_h(x,\tilde{d}) - \eta_{*|x})\right),$$

$$(2.17)$$

where

$$\eta_{*|x} = \varepsilon_* + e_* + \Gamma_{\eta x}\Gamma_x^{-1}(x - x_*) \qquad (2.18)$$

$$\Gamma_{\eta|x} = \Gamma_\varepsilon + \Gamma_e - \Gamma_{\eta x}\Gamma_x^{-1}\Gamma_{x\eta}, \qquad (2.19)$$

and where $\Gamma_{\eta x} = \Gamma_{\varepsilon x} + \Gamma_{ex}$ and $\Gamma_{\eta x} = \Gamma_{x\eta}^{\mathrm{T}}$. When the measurement errors e and parameter x are mutually independent, that is, $\Gamma_{ex} = 0$, we have $\Gamma_{\eta x} = \Gamma_{\varepsilon x}$ in Eqs. (2.17-2.19).

2.3.2 MAP-estimate with approximation error model

The computation of the MAP estimate from the posterior model (2.17) amounts to solving the minimization problem

$$x_{\mathrm{MAP}} = \arg\min\left\{\|\, L_{\eta|x}(y - A_h(x,\tilde{d}) - \eta_{*|x})\,\|^2\right.$$
$$\left. + \|\, L_x(x - x_*)\,\|^2\right\}, \qquad (2.20)$$

where the Cholesky factor $L_{\eta|x}^{\mathrm{T}}L_{\eta|x} = \Gamma_{\eta|x}^{-1}$. Thus, the MAP estimation problem with the approximation error approach is formally similar to the MAP estimation (2.11) with the conventional noise model, and therefore the functional (2.20) can be minimized with the same algorithms as the MAP with conventional noise model (2.11). We refer to the MAP estimate (2.20) as MAP with the *approximation error model* (MAP-AEM).

Note that in the case of non-linear forward models, the mean ε_* and the covariances Γ_ε, $\Gamma_{\varepsilon x}$ and $\Gamma_{x\varepsilon}$ in equations (2.18-2.19) need to be estimated based on Monte Carlo simulations, see Section 2.3.4.

However, this task can be done offline and needs to be done only once for a given measurement setup, and for the expected range of uncertainties.

2.3.3 Complete and enhanced error models

The approximation error model using the mean and covariance defined as in equations (2.18-2.19) is referred as the *complete error model*. While it is clear that ε and x are not independent, it has turned out in several applications that a feasible approximation is obtained by setting $\Gamma_{\varepsilon x} = 0$ and $\Gamma_{x\varepsilon}^{\mathrm{T}} = 0$. With this further approximation, and the earlier assumption $\Gamma_{ex} = 0$, we have

$$\eta_{*|x} \approx \varepsilon_* + e_*, \quad \Gamma_{\eta|x} \approx \Gamma_\varepsilon + \Gamma_e \qquad (2.21)$$

in (2.18-2.19). This approximation is called the *enhanced error model*, see [26,27]. The estimates computed with the enhanced error model were found feasible in several applications, see for example [26,29, 31]. On the other hand, the effect of the approximation in (2.21) was found significant in the deconvolution example in [27].

2.3.4 Computation of the statistics of the approximation error

In cases in which the measurement model is linear and the prior model and measurement error model are Gaussian, the approximation error statistics can be computed analytically, see [26]. In other cases the statistics is, however, typically estimated by Monte Carlo simulation.

For the Monte Carlo simulation, we generate a set of N_s draws from the prior models $\pi(d)$ and $\pi(\bar{x})$. The samples of the unknown $\bar{x}$ and the parameter d are denoted as: $\{\bar{x}^{(\ell)}, d^{(\ell)}, \ell = 1, 2, , \ldots, N_s\}$. These samples are then used for the computation of the *accurate* forward solution $A_\delta(\bar{x}^{(\ell)}, d^{(\ell)})$ and for the *target model* solution $A_h(x^{(\ell)}, \tilde{d})$ for each of the N_s samples. For the computation of the target model solution, the samples $x^{(\ell)}$ are obtained by $x^{(\ell)} = P\bar{x}^{(\ell)}$, see equation (2.14).

Given the accurate and target forward solutions, the samples $\varepsilon^{(\ell)}$ of the approximation error are obtained as

$$\varepsilon^{(\ell)} = A_\delta(\bar{x}^{(\ell)}, d^{(\ell)}) - A_h(P\bar{x}^{(\ell)}, \tilde{d})$$

for the combined unknown nuisance parameter errors and discretization errors. Let ξ denote the stacked variables

$$\xi = \begin{pmatrix} \varepsilon \\ x \end{pmatrix}.$$

The second order joint statistics (the mean ξ_* and covariance matrix Γ_{ξ}) of the approximation error ε and the parameter x are then estimated as

$$\xi_* = \frac{1}{N_s} \sum_{\ell=1}^{N_s} \xi^{(\ell)}, \; \Gamma_{\xi} = \frac{1}{N_s - 1} \sum_{\ell=1}^{N_s} \zeta^{(\ell)} \zeta^{(\ell)\mathrm{T}},$$

where

$$\xi^{(\ell)} = \begin{pmatrix} \varepsilon^{(\ell)} \\ x^{(\ell)} \end{pmatrix}, \; \zeta^{(\ell)} = \begin{pmatrix} \varepsilon^{(\ell)} \\ x^{(\ell)} \end{pmatrix} - \begin{pmatrix} \varepsilon_* \\ x_* \end{pmatrix}$$

and

$$\Gamma_{\xi} = \begin{pmatrix} \Gamma_\varepsilon & \Gamma_{\varepsilon x} \\ \Gamma_{x\varepsilon} & \Gamma_x \end{pmatrix}.$$

The Gaussian approximation for the joint density is written as $\pi(\varepsilon, x) \approx \mathcal{N}(\xi_*, \Gamma_{\xi})$.

2.3.5 Review of earlier work on approximation error theory

The approximation error approach was first proposed for discretization errors with several numerical examples in [26]. The closed form equations for the statistics of the approximation error were derived in the case of the additive linear Gaussian observation model. In this linear case, the approach was evaluated with computed examples of the full angle CT problem and image deblurring problem. The approximation error approach was also applied to non-linear

EIT inverse problem. Since all applications concerned discretization errors, the term "approximation error" is commonly used also where "modelling error" might be a more appropriate term.

In [27], the approximation error approach and discretization errors in linear inverse problems were discussed. The approximation error theory was formulated for both the complete and enhanced error models. The approach was evaluated using a deconvolution example. In this example, the approximations in the enhanced error model produced significant errors and the estimates with the complete error model were better than those with the enhanced error model.

In [29], the approximation error approach was applied for errors due to reduced discretization and truncation of the computation domain. The computed examples concerned a geophysical application of EIT in which the adequately large computation domain leads to prohibitive computation cost. For that reason, the computation domain was truncated near the region of interest and the discretization of the forward model was reduced. It was found that these approximation errors can be efficiently compensated for by using the approximation error approach. It was also shown that only a few samples was adequate for the estimation of the approximation error statistics in this case.

In [30], a circular anomaly in the homogeneous background was estimated using EIT. The CM estimates of the location of the anomaly were computed using MCMC. In these computations, the linear approximation of the EIT forward model was used due to the heavy computation load of repetitive solutions of the full forward problem. The linearization errors were compensated for by using the approximation error approach and feasible estimates of the location of the anomaly were obtained. Erroneous estimates of the location were obtained if the approximation errors due to linearization was not taken into account.

The approximation errors are sometimes reduced by using similar ideas as in the approximation error approach without computing the full statistics of the approximation error. For example,

in [43], an EIT measurement from a target with the known conductivity was conducted and the corresponding forward problem was solved using this conductivity. Then the mean of the observation noise was estimated by computing the difference of the measured and computed voltages. In approximation error approach, this procedure correspond to estimation of the mean of the approximation error by using only one sample.

In addition to EIT, the approximation error approach has also been applied to other inverse problems and other types of (approximation) errors. In optical tomography (OT), model reduction errors were treated in [31]. Significant improvement in the estimate quality was observed when the approximation error approach was used. Furthermore, the performance of the approximation error approach was studied by computing the expected estimation errors by using a simulated data set. The expected estimation errors were computed as sample averages by using the estimated and true absorption and scattering values. The estimation error decreased as the additive measurement noise level decreased when the approximation error approach was employed. On the other hand, the estimation error increased as the additive noise level decreased below the approximation error level when the conventional error model was used. These findings were similar as in the EIT case in [26].

In [33], the approximation errors due to uncertain parameters in the anisotropic forward model were compensated for by using approximation error approach. The strength and direction of the anisotropy was modeled with a few parameters and the approximation error statistics were computed using a prior distribution of these parameters. In [34], the shape of the target boundary in OT measurements was unknown and therefore the reconstructions were computed using a model domain. Although the actual medium was isotropic, the discrepancy between the model and the reality could be interpreted as generation of anisotropies. However, the direction and strength of the anisotropy was unknown also in this case and therefore this uncertainty was modeled with approximation error approach similarly as in [33]. Feasible esti-

mates were obtained by employing the approximation error approach, while the reconstructions with the conventional measurement error model were useless.

The compensation of errors due to reduced discretization and truncation of the computation domain in OT was studied in [32]. The approach was evaluated with laboratory measurements from a cylindrical target. In the reduced model, the computation domain was truncated near the measurement sensors. Feasible estimates were obtained using the approximation error approach when the reduced model was used. The reconstructions with the conventional error model were infeasible when the same forward model was used.

The approximation errors in OT due to a approximative mathematical model for light propagation in the medium and model reduction were discussed in [35]. In that work, the computationally tedious radiative transfer model was approximated with the diffusion model. The diffusion model cannot describe light propagation accurately in weakly scattering medium and near the collimated light sources and the boundary of the computation domain. It was found that the approximation error approach compensates efficiently both errors due to incorrect forward model and model reduction.

In [44], the approximation error approach was used to compensate for errors due to first order Born approximation with an infinite space Green's function model in OT. In reality, the forward model is nonlinear and data is generated on a finite domain with possibly unknown background properties. It was shown that feasible estimates can be produced by using linear reconstruction method and the approximation error approach also in situations in which the background optical properties are not known and a reference measurement is not available.

In OT, the absorption coefficient is usually more interesting than the scattering coefficient. In order to get reliable estimates of the absorption, the scattering coefficient has to be known or estimated simultaneously with the absorption. In [28], the scattering coef-

ficient was approximated with an homogeneous value in inverse computations and the approximation errors were treated with the approximation error approach. In general terms, this procedure can be thought as approximate premarginalization of uninteresting distributed parameters. When the uninteresting parameters are premarginalized, the resulting inverse problem is computationally more feasible than estimation of all coefficients.

The extension and application of the approximation error approach to time-dependent linear inverse problems was considered in [45] and to non-linear inverse problems in [46]. In these papers, both approximation errors due to a reduced forward model and increased time stepping in the evolution model were taken into account. In [47], the approximation error approach and discretization errors due to spatial discretization were studied. In that work, the temporal discretization of the model was exact as it was represented using an analytic semi-group. In [48], the approximation error approach for large dimensional non-stationary inverse problems was proposed. An application of the approach for estimation of the distributed thermal parameters of tissue was represented. The approximation error approach in non-stationary inverse problems was modified to allow the updating of the approximation error statistics during the accumulation of the measurement information in [49]. The updating of the statistics was accomplished by computing weights for the approximation error samples using the measured data. The approximation error statistics was then computed as weighted sample average after each measurement.

In [50], the identification of a contaminant source in a lake environment by using remote sensing measurements was discussed. The objective was to determine the location, release rate and the time instant at which the release was started. The discretization errors due to forward model reduction were taken into account by employing the approximation error approach. The estimated approximation error statistics revealed the accumulation of the discretization errors with time (seen as increasing error levels). It was found that large errors of the estimated location of the pollution

source occurs if the approximation errors are not modeled. The location of the release was accurately found when the approximation error approach was used. Furthermore, the confidence limits with the approximation error approach were feasible.

In [51], the flow of the electrically conductive fluids in porous media was imaged using EIT. The approximation error approach was used for compensation of errors due to model reduction and uncertain parameters (permeability distribution) in the evolution model. The estimates of the water saturation distributions were significantly improved when the approximation error approach was used.

In [52], the non-stationary concentration distribution was reconstructed using EIT. The actual time dependent velocity field of the flow was unknown and the mean flow was used in the evolution model. The approximation error approach was used to compensate for errors due to time variability of the velocity field. This approach was extended in [53] in which the simultaneous estimation of the concentration and a reduced order approximation for the unknown non-stationary velocity field was proposed. The approximation errors due to non-estimated part of the velocity field were treated using the approximation error approach.

In [54], the non-stationary approximation error approach was experimentally evaluated with three-dimensional process tomography measurements. Electrical impedance tomography measurements were conducted in case of rapidly moving fluid in a pipeline. The approximation errors due to truncation of the computation domain, reduced discretization, unknown contact impedances, and partially unknown boundary condition in the convection-diffusion model were taken into account using approximation error approach. The reconstructions using approximation error approach were superior compared to stationary reconstructions and non-stationary reconstructions without the approximation error approach.

3 Electrical impedance to-mography

In electrical impedance tomography (EIT), N_{el} contact electrodes e_ℓ are attached on the boundary of the object, see figure 3.1. Currents are injected through these electrodes and the resulting voltages are measured using the same electrodes. The conductivity σ of the object is estimated based on the measured voltages and known currents.

In Section 3.1, the forward model and the numerical implementation of the model are explained. The forward model describes how the voltages on the electrodes can be determined when the conductivity of the object and the injected currents are known. In this thesis, the complete electrode model is used as the forward model [55, 56]. The forward problem is solved with the finite element method. The notations used in the finite element approximations are explained in Section 3.1. Furthermore, the measurement error model is also represented in Section 3.1. In Section 3.2, the inverse problem in EIT is briefly reviewed. In Section 3.3, the computed estimates and prior model in this thesis are discussed. For more detailed discussions on EIT, see for example [57–59].

3.1 FORWARD MODEL AND NOTATION

We model the EIT measurements with the complete electrode model [55, 56]:

$$\nabla \cdot \sigma(x)\nabla u(x) = 0, \quad x \in \Omega \tag{3.1}$$

$$u(x) + z_\ell \sigma(x)\frac{\partial u(x)}{\partial n} = U_\ell, \quad x \in e_\ell \subset \partial\Omega, \tag{3.2}$$

$$\int_{e_\ell} \sigma(x)\frac{\partial u(x)}{\partial n}\, dS = I_\ell, \quad x \in e_\ell \subset \partial\Omega, \tag{3.3}$$
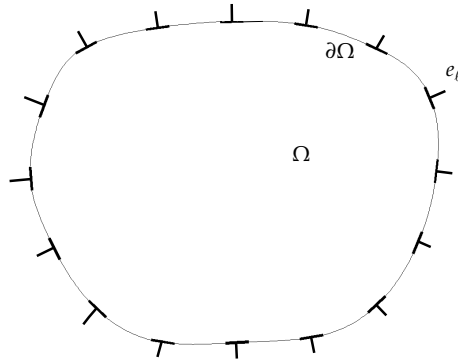
Figure 3.1: A schematic representation of an EIT experiment. The contact electrodes e_ℓ are attached on the boundary $\partial\Omega$ of the body Ω.

$$\sigma(x)\frac{\partial u(x)}{\partial n} = 0, \quad x \in \partial\Omega \setminus \bigcup_{l=1}^{N_{\text{el}}} e_\ell. \tag{3.4}$$

where $\Omega \subset \mathbb{R}^q$, $\quad q = 2,3$, denote the measurement domain, $x \in \mathbb{R}^q$ is the position vector, $u(x)$ is the potential distribution inside Ω, n is the outward unit normal vector at $\partial\Omega$, $\sigma(x)$ is the conductivity, and z_ℓ is the contact impedance between the object and the electrode e_ℓ. The currents satisfy the charge conservation law

$$\sum_{\ell=1}^{N_{\text{el}}} I_\ell = 0, \tag{3.5}$$

and a ground level for the voltages can be fixed by

$$\sum_{\ell=1}^{N_{\text{el}}} U_\ell = 0. \tag{3.6}$$

3.1.1 Finite element approximation of the forward model

The numerical approximation of the forward model (3.1-3.6) is based on the finite element (FEM) approximation. In the FEM approximation, the domain Ω is divided into N_e disjoint elements joined at N_n vertex nodes. The potential u and electrode potentials $U \in \mathbb{R}^{N_{\text{el}}}$ satisfying the variational form (see [56]) of (3.1-3.6) are approximated

as

$$u^h(x) = \sum_{i=1}^{N_n} \alpha_i \phi_i(x), \tag{3.7}$$

$$U^h = \sum_{j=1}^{N_{el}-1} \beta_j n_j \tag{3.8}$$

where the functions ϕ_i are the nodal basis functions of the finite element mesh and vectors $n_j \in \mathbb{R}^{N_{el}}$ are chosen such that condition (3.6) holds. The parameter h denotes the size of the largest element in the mesh and defines the discretization level. The theory of elliptic operators guarantees that [56]

$$(u^h(x), U^h) \to (u(x), U) \text{ as } h \to 0 \quad \text{and } N_n \to \infty$$

where $(u(x), U)$ is the solution of the variational formulation of (3.1-3.6). The conductivity $\sigma(x)$ is approximated in a basis

$$\sigma(x) = \sum_{k=1}^{N} \sigma_k \psi_k(x). \tag{3.9}$$

Typically, $\psi_k(x)$ are the nodal basis functions in a separate finite element type mesh. In the following, we identify the conductivity $\sigma(x)$ in (3.9) with the coefficient vector $\sigma = (\sigma_1, \ldots, \sigma_N)^{\mathrm{T}} \in \mathbb{R}^N$. By these choices, the numerical forward solution for each current injection is obtained by solving a $(N_n + N_{el} - 1) \times (N_n + N_{el} - 1)$ system of equations. For further details on the FEM approximation of the complete electrode model, see for example [2, 60].

3.1.2 Conventional error model in EIT

The measurement noise in EIT experiments is commonly modeled as Gaussian additive noise which is mutually independent with the unknown conductivity. This leads to measurement model

$$V = U_h(\sigma, d) + e, \quad e \sim \mathcal{N}(e_*, \Gamma_e) \tag{3.10}$$

where $V \in \mathbb{R}^m$ is the vector of the measured voltages, $U_h(\sigma, d) \in \mathbb{R}^m$ is the forward solution corresponding to single EIT experiment,

h is the discretization level parameter in (3.7), $\sigma \in \mathbb{R}^N$ is the conductivity vector, and $e \in \mathbb{R}^m$ is a Gaussian distributed measurement noise with mean $e_* \in \mathbb{R}^m$ and covariance matrix Γ_e. Furthermore, the parameter vector d represents (possibly unknown) nuisance parameters in the forward model. Typical nuisance parameters in EIT are the contact impedances and parameters that define the shape of the computation domain, for example.

3.2 INVERSE PROBLEM IN EIT

In this section, a brief review of inversion methods in EIT is given. The absolute imaging is discussed in Section 3.2.1 and difference imaging in Section 3.2.2. For more extensive reviews of the EIT reconstruction methods, see [1–3, 57–59, 61, 62]. For the mathematical background of the EIT inverse problem, see [63] in which the EIT inverse problem was first formulated. Since then uniqueness and existence proofs for the EIT inverse problem with different regularity requirements on the conductivity have been represented in [64–66], for example.

In this thesis, the conductivity is assumed to be stationary during the acquisition of one measurement frame both in absolute imaging and in difference imaging. For the treatment of non-stationary EIT problem, see for example [67–69].

3.2.1 Absolute imaging

Most of the EIT reconstruction methods are based on the regularized non-linear least squares (LS) formulation of the EIT inverse problem, see for example [70–73]. The solution of the inverse problem in this case corresponds to minimization of the functional

$$\|L_1(V - U_h(\sigma, d) - e_*)\|^2 + \alpha \|L_2(\sigma - \sigma_*)\|^2 \qquad (3.11)$$

with respect σ. The interpretation of the terms in (3.11) is different depending on the inversion method used. For example, in Tikhonov regularization L_1 is a weighting matrix, α is the regularization parameter, L_2 is the regularization matrix and σ_* is a prior

estimate for the conductivity. In statistical framework, the functional of the form (3.11) corresponds to Gaussian models for the noise and prior. In this case, the matrix $L_1 = L_e$ is the Cholesky factor such that $\Gamma_e^{-1} = L_e^{\mathsf{T}} L_e$, $\sqrt{\alpha} L_2 = L_\sigma$ such that $\Gamma_\sigma^{-1} = L_\sigma^{\mathsf{T}} L_\sigma$ and σ_* is the mean of the Gaussian prior. The solution of the minimization problem (3.11) can be computed using minimization algorithm such as Gauss-Newton algorithm.

Note that significant reconstruction errors occur in many practical applications if discretization of the forward problem is reduced or the nuisance parameter vector d is unknown.

3.2.2 Difference imaging

In absolute imaging the conductivity σ is reconstructed based on the measured voltages V corresponding to single time instant. On the other hand, in (time) difference imaging the difference in the conductivity between two time instants is reconstructed. The first step in difference imaging is to measure the reference measurement V_{ref} corresponding to conductivity σ_{ref}. Then the actual measurement V corresponding to conductivity σ is conducted and the difference $\delta\sigma = \sigma - \sigma_{\text{ref}}$ is reconstructed.

The reconstruction of the conductivity $\delta\sigma$ in difference imaging is based on the linearized observation model

$$V \approx U(\sigma_{\text{ref}}, d) + J(\sigma - \sigma_{\text{ref}}) + e, \tag{3.12}$$

where J is the Jacobian matrix (sensitivity matrix) of the forward map evaluated at σ_{ref}. The observation model (3.12) is also used in absolute imaging when the functional (3.11) is minimized by computing only one step of the minimization algorithm. One such algorithm is the NOSER algorithm [74]. In difference imaging, the forward solution $U(\sigma_{\text{ref}}, d)$ is replaced with measured reference voltage V_{ref}. In this case, the observation model is of the form

$$\underbrace{V - V_{\text{ref}}}_{\delta V} \approx J \underbrace{(\sigma - \sigma_{\text{ref}})}_{\delta\sigma} + e. \tag{3.13}$$

The difference in conductivity $\delta\sigma$ can be reconstructed under the model (3.12) by regularized least squares framework, see [16] for example. Other methods that fall under the formalism of (3.12) are back-projection methods [75,76] and sensitivity coefficient methods [77].

The difference imaging is to some extent tolerant to approximation errors since absolute errors in the measured voltages are partially canceled when the difference of the measurements is computed. Due to this property the difference imaging has been favoured over absolute imaging. Difference imaging has been applied to the monitoring of the industrial processes [16,78] and monitoring of patients in clinical applications [7,79], for example. However, the feasibility of the difference imaging is questionable in several applications. The reference measurement is not often available or the interesting chance in the conductivity have occurred prior to the reference measurement. Furthermore, the absolute conductivity values cannot be obtained and the estimates are inaccurate if the actual difference in conductivities is large. The unknown nuisance parameters d are also a problem in difference imaging.

3.3 COMPUTED ESTIMATES AND PRIOR MODEL

In this thesis, EIT inverse problem is solved using the Bayesian inversion approach reviewed in general formalism in Chapter 2. In Section 3.3.1, the Bayesian estimates to be computed in this thesis are represented and in Section 3.3.2 the prior model is represented.

3.3.1 Computed estimates

The first estimate to be computed is the MAP-estimate with the conventional error model (2.11):

$$
\begin{aligned}
\sigma_{\text{MAP}} &= \arg\max_{\sigma \geq 0} \pi(\sigma \mid V) \\
&= \arg\min_{\sigma \geq 0} \left\{ \|L_e(V - U_h(\sigma, d) - e_*)\|^2 \right. \\
&\quad \left. + \|L_\sigma(\sigma - \sigma_*)\|^2 \right\}.
\end{aligned}
\tag{3.14}
$$

Note that the nuisance parameter d may or may not correspond to actual value of the parameter when this estimate is computed. Furthermore, this estimate may be computed using accurate or coarse discretization.

As a second estimate the MAP-AEM estimate (2.20) is computed. The MAP-AEM estimate (2.20) with EIT notations becomes

$$\sigma_{\text{MAP}} = \arg \min_{\sigma \geq 0} \left\{ || \ L_{\eta|\sigma}(V - U_h(\sigma, \tilde{d}) - \eta_{*|\sigma}) \ ||^2 \right.$$
$$\left. + \ || \ L_\sigma(\sigma - \sigma_*) \ ||^2 \right\}. \tag{3.15}$$

Note that the minimization problems (3.14) and (3.15) are of similar form than the general regularized LS solution (3.11), and therefore the functional (3.15) can be minimized using standard algorithms used in regularized LS minimization problems. In this thesis, Gauss-Newton algorithm is used.

3.3.2   Prior model

In this thesis, a proper Gaussian smoothness prior model $\pi(\sigma)$ is constructed similarly as in [26, 31, 32]. In the construction of the prior model, the conductivity is considered in the form

$$\sigma(x) = \sigma_{\text{in}}(x) + \sigma_{\text{hg}}(x)$$

where $\sigma_{\text{in}}(x)$ is a spatially inhomogeneous conductivity with zero mean, and $\sigma_{\text{hg}}(x)$ is a spatially homogeneous conductivity of nonzero mean. For the latter, we can write $\sigma_{\text{hg}}(x) = c\mathbb{I}$, where $\mathbb{I} \in \mathbb{R}^N$ is a vector of ones and $\mathbb{R} \ni c \sim \mathcal{N}(\sigma_*, \mu_{\text{hg}}^2)$. The inhomogeneous part of the conductivity is modeled as $\sigma_{\text{in}} \sim \mathcal{N}(0, \Gamma_{\text{in}})$. We model σ_{in} and c as mutually independent, that is, with respect to the prior model, the background conductivity is modeled mutually independent with the inhomogeneities in the conductivity.

In practice, the homogeneous background σ_* and the standard deviation μ_{hg} are set using our prior information of the target. Furthermore, the prior covariance Γ_{in} is constructed by choosing the

variance of elements μ_{in}^2 (diagonal elements of Γ_{in}) and the correlation length. The correlation length expresses roughly our prior estimate about the expected size of the inhomogeneities in the medium. This also means that in the model for σ_{in}, any two elements that correspond to spatial locations that are further away from each other than the correlation length, are (approximately) mutually independent.

Thus, we have the prior covariance $\Gamma_\sigma = \Gamma_{\text{in}} + \mu_{\text{hg}}^2 \mathbb{I}\mathbb{I}^{\text{T}}$ and

$$\pi(\sigma) = \mathcal{N}(\sigma_* \mathbb{I}, \Gamma_\sigma).$$

This prior model is a proper distribution, in that the covariance exists in the first place.

Traditional smoothness prior models are improper, that is, the variances are infinite, and samples cannot be drawn from such distributions. The approximation error approach, on the other hand, is based on computing the statistics of ε over the prior distribution. This is not possible with a prior of unbounded variances. In the statistical framework, sophisticated non Gaussian prior models for the conductivity can also be constructed. For more information on the non Gaussian prior models, see for example [2, 61].

4 Review on the results

In this chapter, a brief review of the results obtained in Publications I-IV is given.

4.1 PUBLICATION I: DISCRETIZATION ERRORS AND ERRORS DUE TO PARTIALLY UNKNOWN GEOMETRY

The motivation of this research originated from a process tomography application in which the height of the liquid in a process tank can change over time. In this case, one approach for eliminating the errors due to unknown height of the liquid is to estimate the free surface between the air and the liquid simultaneously with the conductivity [80,81]. This approach increases the computational load and requires accurate discretization of the forward problem. However, in process tomography the measurements are often done with high frame rates and the reconstructions also have to be computed in limited time. Therefore, the reconstructions are often computed using coarse discretization of the forward model and the shape of the target is not estimated. The coarse discretization and erroneous computation domain have been shown to produce significant reconstruction errors, see [26] and [82]. In this work, both of these errors are taken into account by using the approximation error approach.

4.1.1 Measurement configuration

In order to evaluate the approximation error approach, the measurements were conducted using a cylindrical measurement tank; the radius and height of the tank were 20 cm and 52 cm, respectively. Eighty equally spaced stainless steel electrodes were attached around the surface of the tank such that they were in five different layers. The electrode layers are denoted by thick red lines on the boundary in Figure 4.1. The height of the computation domain $\tilde{\Omega}$ used in the inverse computation was chosen to be 46 cm.

Before the measurements the measurement tank was filled with tap water; the height of the water level was 42 cm. The difference (4 cm) between the height of the water level and the computation domain $\tilde{\Omega}$ is also denoted in Figure 4.1.

4.1.2 Computation of the approximation error statistics

The approximation error statistics due to unknown height of the liquid and reduced discretization was estimated using methods in Section 2.3.4. In this work, the approximation errors due to discretization and unknown height of the liquid were separated. In this case, the accurate observation model is written in the form

$$V = U_h(\sigma, \tilde{d}) + \underbrace{[U_\delta(\bar{\sigma}, d) - U_\delta(\bar{\sigma}, \tilde{d})]}_{\varepsilon_1} + \underbrace{[U_\delta(\bar{\sigma}, \tilde{d}) - U_h(\sigma, \tilde{d})]}_{\varepsilon_2} + e,$$

(4.1)

where ε_1 is the approximation error due to inaccurate computation domain and ε_2 is the approximation error due to reduced discretization, d is the height of the liquid in the process tank (and the height of the accurate computation domain), $\tilde{d} = 46$cm is the height of the computation domain $\tilde{\Omega}$ in inverse computations.

The samples of the approximation error ε_1 were obtained as

$$\varepsilon_1^{(\ell)} = U_\delta(\bar{\sigma}^{(\ell)}, d^{(\ell)}) - U_\delta(\bar{\sigma}^{(\ell)}, \tilde{d}).$$

(4.2)

The height of the liquid d was modeled to be equally distributed between 41 cm and 52 cm. The forward problems $U_\delta(\bar{\sigma}^{(\ell)}, d^{(\ell)})$ were computed using 12 different meshes which heights were $d^{(\ell)} = 41$, 42,. . ., 52 cm. This corresponds to sample size $N_s = 12$. The samples of the conductivity $\bar{\sigma}^{(\ell)}$ were the same homogeneous sample $\bar{\sigma}^{(\ell)} = \sigma_{\mathrm{hg}}$ for all N_s samples.

The samples of the approximation error ε_2 were obtained as

$$\varepsilon_2^{(\ell)} = U_\delta(\bar{\sigma}^{(\ell)}, \tilde{d}) - U_h(P\bar{\sigma}^{(\ell)}, \tilde{d}),$$

(4.3)

where all forward problem solutions were computed using computation domain $\tilde{\Omega}$. The number of samples was in this case $N_s = 1$

and the mean of the discretization error was estimated based on one homogeneous sample $\bar{\sigma}^{(\ell)} = \sigma_{\mathrm{hg}}$.

The total approximation error ε is obtained as $\varepsilon = \varepsilon_1 + \varepsilon_2$. Both ε_1 and ε_2 were modeled to be Gaussian random variables and enhanced error model was used. In this case, the mean and covariance matrix of the approximation errors due to partially unknown geometry and reduced discretization are $\varepsilon_* = \varepsilon_{1*} + \varepsilon_{2*}$ and $\Gamma_\varepsilon = \Gamma_{\varepsilon_1} + \Gamma_{\varepsilon_2}$. The covariance matrix $\Gamma_{\varepsilon_2} = 0$ since we used only one sample for the estimation of the statistics of the discretization error and the covariance matrix could not be estimated.

4.1.3 Results

The location of two plastic rods inside the measurement tank is denoted in Figure 4.1. All conductivity estimates were computed using the inverse mesh, height 46 cm. The estimates of the conductivity distribution are shown in Figure 4.1.

The difference reconstruction is shown in the upper right Figure 4.1. The reference measurement V_{ref} was done when the water level was 46 cm and there was only water in the tank, and the actual measurement V was the same as in the absolute reconstructions. The MAP-AEM estimate is shown in bottom left figure. In this reconstruction only the discretization error statistics was taken into account. Reconstruction errors can be seen in both the difference and absolute reconstructions. The errors can be seen mainly near the surface of the water in both figures.

The MAP-AEM estimate shown in the bottom right Figure 4.1 was computed using the approximation error approach, and both the discretization and modelling error due partially unknown geometry were taken into account. As can be seen, errors due to both the discretization error and error due to partially unknown geometry can be reduced simultaneously. Furthermore, results demonstrate that the reconstruction errors due to discretization errors can be reduced effectively using the mean of the discretization error based on one sample.
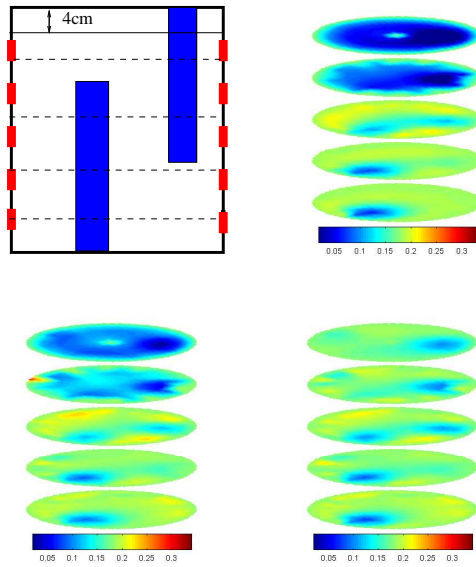
Figure 4.1: Upper left: the measurement configuration viewed from the side. The dashed lines denote the heights of the visualization layers 6, 16, 26, 36, 46 cm. Two plastic rods and electrodes on the boundary are shown. The difference (4 cm) between the height of the inverse mesh (46 cm) and the height of the water level (42 cm) is denoted in the figure. Upper right: the difference reconstruction. Bottom left: the conductivity distribution computed using the approximation error approach; only the discretization error is taken into account. Bottom right: the conductivity distribution computed using the approximation error approach; both the discretization error and the geometrical modelling error are taken into account.

4.2 PUBLICATION II: ERRORS DUE TO DISCRETIZATION, MODEL REDUCTION AND UNKNOWN CONTACT IMPEDANCES

Most of the current approaches to EIT treat the contact impedances as known, fixed parameters. However, in practical measurements they are always unknown and can change during the measurements. One possible approach is to estimate the contact impedances simultaneously with the conductivity [83,84]. The errors due to unknown contact impedances have been studied in [85], and it was shown that severe reconstruction errors result if the contact impedances are not modeled accurately.

In this section, we employ approximation error approach for errors due to reduced discretization and unknown contact impedances. For the results concerning also errors due to truncation of the computation domain, see Publication II.

4.2.1 Measurement configuration

The measurement target was a cylindrical measurement tank, see top left Figure 4.2. The radius and height of the cylindrical tank were 14 cm and 7 cm, respectively. Sixteen equally spaced electrodes were attached to the boundary of the tank. Fifteen trigonometric current patterns were used, and the voltages were measured between adjacent electrodes. The measurement tank was filled with tap water and a plastic rod was placed into the water near electrode 1. The diameter of the rod was 5 cm. To simulate the variation of the contact impedances, vaseline was brushed on to the surface of electrodes 1 and 3.

4.2.2 Computation of the approximation error statistics

Statistics of the approximation error due to discretization and unknown contact impedances were estimated as in Section 2.3.4. The samples of the approximation error in the case of reduced dis-

cretization and unknown contact impedances were obtained as

$$\varepsilon^{(\ell)} = U_\delta(\bar{\sigma}^{(\ell)}, z^{(\ell)}) - U_h(P\bar{\sigma}^{(\ell)}, \tilde{z}). \tag{4.4}$$

The samples of the approximation errors in the case of approximation errors due to unknown contact impedances were computed as

$$\varepsilon^{(\ell)} = U_\delta(\bar{\sigma}^{(\ell)}, z^{(\ell)}) - U_\delta(\bar{\sigma}^{(\ell)}, \tilde{z}). \tag{4.5}$$

The prior model for contact impedances was a gamma distribution. Furthermore, the contact impedances were modelled as mutually independent and identically distributed variables. The rationale for choosing this skewed distribution model for the elements of z was to choose a model that (i) has most of the probability mass on small (positive) values and (ii) has a long tail in the larger positive values. This (ad hoc) choice models (roughly) the fact that the contact impedances in measurement tanks and process vessels are usually relatively close to zero for clean electrodes but may have significantly larger values for contaminated electrodes.

The samples of the contact impedances $z^{(\ell)}$ were drawn from the prior model. The 'inaccurate' forward problems $U_h(P\bar{\sigma}^{(\ell)}, \tilde{z})$ and $U_\delta(\bar{\sigma}^{(\ell)}, \tilde{z})$ were computed using an approximative contact impedance $\tilde{z}$ which was in this case the mean of the prior model. The samples of the conductivity $\bar{\sigma}^{(\ell)}$ were drawn from a proper Gaussian smoothness prior.

4.2.3 Results

The MAP-CEM reconstruction with the forward model $U_h(\sigma, \tilde{z})$ is shown in middle left Figure 4.2. Discretization errors and errors due to unknown contact impedances have caused reconstruction errors near the boundary of the tank. The MAP-CEM reconstruction with the forward model $U_\delta(\sigma, \tilde{z})$ is shown in middle right Figure 4.2. In this reconstruction, the reconstruction errors are more severe than when coarse discretization of the forward model was used. The MAP-CEM estimate with the estimated contact impedances (forward model $U_\delta(\sigma, z_{\text{est}})$) is shown in bottom left figure.

This estimate serves as the reference estimate with the conventional noise model when the contact impedances are estimated and accurate discretization is used [83,84,86]. The MAP-AEM reconstruction with the forward model $U_h(\sigma, \tilde{z})$ is shown in bottom right figure.

As can be seen in Figure 4.2, the MAP-CEM reconstruction with the forward model $U_\delta(\sigma, z_{\text{est}})$ is similar to the MAP-AEM reconstruction with the model $U_h(\sigma, \tilde{z})$. This indicates that discretization errors and errors due to unknown contact impedances can be compensated efficiently for by the approximation error approach. The computation time of MAP-AEM reconstruction was only 0.78% of that of MAP-CEM reconstruction with estimated contact impedances. Furthermore, the computation of the MAP-AEM estimate is less complicated since contact impedances does not have to be estimated.

4.3 PUBLICATION III: ERRORS DUE TO UNKNOWN DOMAIN BOUNDARY

The inaccurate knowledge of the shape of the target body is a major problem in biomedical EIT. Most of the available reconstruction methods assume that the boundary of the target body is known. As an example, consider EIT measurements of pulmonary function from the surface of the thorax. In principle, the shape of the patient's thorax could be obtained from other imaging modalities such as computerized tomography (CT) or magnetic resonance imaging (MRI). However, such information is often not available and therefore the reconstruction has to be computed using an approximate model domain. The use of an incorrect model domain has been shown to produce severe errors in the reconstructed conductivity images, see [85,87–89].

There are a few distinct approaches to compensate for the errors caused by inaccurately known boundary. The method proposed in [90,91] eliminates the errors caused by inaccurately known boundary in 2D EIT by using the theory of Teichmuller mappings. The extension of the method to 3D EIT was considered in [86]. Si-
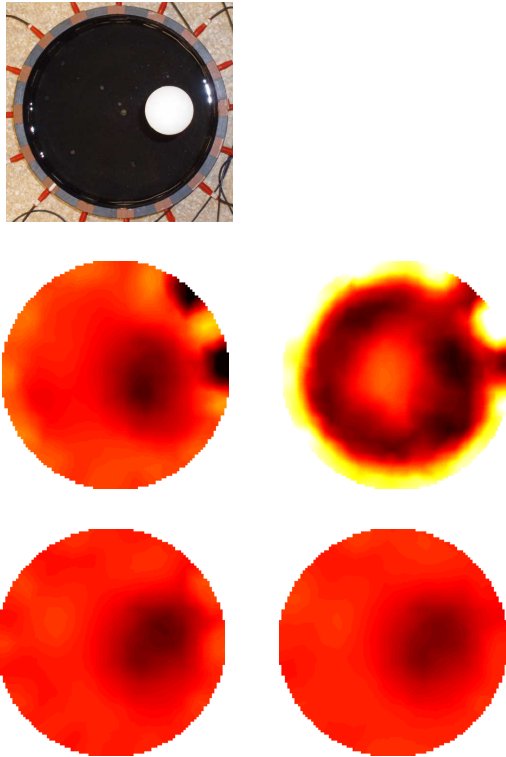
Figure 4.2: Top: The photograph of the measurement set-up. Middle left: The MAP-CEM estimate with forward model $U_h(\sigma, \tilde{z})$ Middle right: The MAP-CEM estimate with forward model $U_\delta(\sigma, \tilde{z})$. Bottom left: MAP-CEM estimate with with forward model $U_\delta(\sigma, z_{\text{est}})$. Bottom right: The MAP-AEM estimate with forward model $U_h(\sigma, \tilde{z})$.

multaneous reconstruction of the conductivity and electrode movement have been proposed for difference imaging in [92, 93]. These approaches are based on a linearized perturbation model and have been evaluated only for relatively small movements of the boundary between the measurement states. Recently, it has been demonstrated that the so called D-bar method (see e.g [94]), which is a direct method based on a constructive uniqueness proof for two-dimensional (2D) EIT [65], has some tolerance against domain modeling errors [95].

In this section, the approximation errors due to unknown domain boundary and reduced discretization were reduced by employing the approximation error approach. The numerical results are computed both with enhanced and complete error model. In Publication III, the enhanced error model was used. Note that, the numerical results in Publication III were computed based on simulated and real measurements. In this section, the numerical results are computed based on simulated data in order to compute reconstruction error estimates. The same simulated measurements were used in this section as in Publication III.

4.3.1   Computation of the approximation error statistics

Statistics of the approximation error due to discretization and unknown shape of the boundary were estimated as in Section 2.3.4. The samples of the approximation error due to unknown domain boundary and reduced discretization were obtained as

$$\varepsilon^{(\ell)} = U_\delta(\bar{\sigma}^{(\ell)}, \gamma^{(\ell)}) - U_h(\sigma^{(\ell)}, \tilde{\gamma}), \qquad (4.6)$$

where $\gamma^{(\ell)}$ is the parameterization of the boundary of the domain $\Omega^{(\ell)}$ and $\tilde{\gamma}$ is the parameterization of the boundary of the model domain $\tilde{\Omega}$ that is used in the inverse problem. In this case, the model domain $\tilde{\Omega}$ is a circular domain with diameter ρ.

The samples of the approximation error due to pure domain boundary errors were obtained as

$$\varepsilon^{(\ell)} = U_\delta(\bar{\sigma}^{(\ell)}, \gamma^{(\ell)}) - U_\delta(\sigma^{(\ell)}, \tilde{\gamma}). \qquad (4.7)$$

The relation of the representation of the conductivities $\bar{\sigma}$ and σ is of the form $\bar{\sigma}(x) = \sigma(T(x))$, where

$$T : \Omega \mapsto \tilde{\Omega} \tag{4.8}$$

is a mapping that models the deformation of domain Ω to $\tilde{\Omega}$. Obviously, the true deformation T between the measurement domain and model domain is not known, and one has to choose a model for the deformation. In the numerical examples considered in this study T is chosen such that the angle and relative distance (between the center of the domain and the boundary) of a co-ordinate point is preserved. Although this simple deformation model seems to work well with the test cases we have considered, we note that other transformation models may be used as well. More advanced choices for the transformation model can be sought for from the literature of image registration, see e.g. [96]. The deformation of the conductivity can be represented by a linear transformation

$$P\bar{\sigma} = \sigma, \tag{4.9}$$

where P is a matrix that interpolates the nodal conductivity (see (3.9)) in Ω into a nodal conductivity in $\tilde{\Omega}$ according to the deformation T.

For the construction of the prior model $\pi(\gamma)$ for generation of the samples $\gamma^{(\ell)}$, 150 chest CT images were segmented and samples of the boundary parameters were obtained. The sample based Gaussian approximation for the prior model $\pi(\gamma)$ was constructed. The samples $\gamma^{(\ell)}$ corresponding to sample domains $\Omega^{(\ell)}$ were drawn from the prior model $\pi(\gamma)$ and the samples of the conductivity $\bar{\sigma}^{(\ell)}$ were drawn from a proper Gaussian smoothness prior. The number of the samples was $N_s = 1000$.

To compute the target models $U_\delta(\sigma^{(\ell)}, \tilde{\gamma})$ and $U_h(\sigma^{(\ell)}, \tilde{\gamma})$, the conductivity samples were mapped from $\Omega^{(\ell)}$ to model domain $\tilde{\Omega}$ by

$$\sigma^{(\ell)} = P^{(\ell)}\bar{\sigma}^{(\ell)}, P^{(\ell)} : \Omega^{(\ell)} \mapsto \tilde{\Omega},$$

where $P^{(\ell)} = P^{(\ell)}(\gamma^{(\ell)}, \rho)$ is a matrix that interpolates nodal conductivity from $\Omega^{(\ell)}$ to $\tilde{\Omega}$ according to the deformation T, see (4.9).

Note that in this section the number of samples N_s is higher than in Publication III. In Publication III, the explicit prior model $\pi(\gamma)$ was not constructed and the statistics of the approximation error was computed using the 150 CT samples. However, we we have noticed that in the case of the complete error model the 150 samples is not enough since the convergence of the estimates of the covariances $\Gamma_{\sigma\varepsilon}$ and Γ_σ require more samples.

4.3.2 Results

The actual conductivity σ_{true} is shown in top left Figure 4.3. The conductivity of lungs, background and heart are 1.2, 2 and 3.6 (arbitrary units), respectively.

The reconstructions in Figure 4.3 were computed using the forward model $U_\delta(\sigma, \tilde{\gamma})$, i.e. accurate discretization was used in all reconstructions. Thus in this section the pure domain modeling errors are investigated, for the results concerning simultaneous discretization errors and domain modeling errors, see Publication III.

The MAP-CEM reconstruction computed using the circular model domain $\tilde{\Omega}$ is shown in Figure 4.3. This reconstruction show intolerable errors. The MAP-AEM reconstructions with the enhanced and complete error models are shown in bottom left and bottom right Figure 4.3, respectively. As can be seen, significant improvement in the image quality is obtained by employing the approximation error approach. The shape of the organs in MAP-AEM reconstructions are similar but the contrast is better in that computed with the complete error model.

The computation times and relative estimation errors Δ_σ for different estimates are shown in table 4.1. The relative estimation error is computed as

$$\Delta_\sigma = \frac{\| P\sigma_{\text{true}} - \sigma \|}{\| P\sigma_{\text{true}} \|} \cdot 100\% \tag{4.10}$$

As can be seen, the computation times of the MAP-AEM estimates are almost equal. The relative estimation error of the MAP-AEM estimates are lower than that of MAP-CEM estimate. The relative

estimation error of the MAP-AEM estimate with the complete error model is smaller than that of MAP-AEM with the enhanced error model. This is due to the fact that the estimated conductivity values of the MAP-AEM with the complete error model are closer to the actual values of the conductivity. Feasible reconstructions can be obtained using the approximation error approach with both the enhanced and complete error models.

Table 4.1: *The relative estimation errors Δ_σ (equation (4.10)) and computation times for different reconstructions.*

Estimate	Error model	Δ_σ	Time (s)
MAP-CEM	conventional	35.5	60.9
MAP-AEM	enhanced	21.9	50.8
MAP-AEM	complete	15.4	49.1

4.4 PUBLICATION IV: APPROXIMATIVE RECOVERY OF THE SHAPE OF THE OBJECT

In the fourth publication, the approximative recovery of the shape of the body based on the EIT measurements is proposed. The approximation error approach is employed in a novel way in which a low rank approximation for unknown approximation error is estimated simultaneously with the conductivity. After the estimation of the approximation error, the shape of the target body is estimated by using an approximate joint distribution model of the approximation error and the boundary parameterization. Furthermore, the confidence limits of the estimated boundary parameterization are computed.

4.4.1 Measurement configuration

The measurement phantom is shown in Figure 4.4. The phantom consist of measurement tank filled with saline and agar organs. The
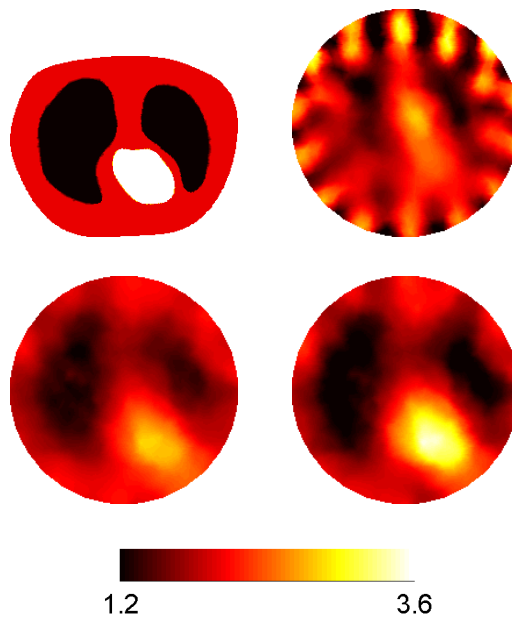
Figure 4.3: Upper left: The actual conductivity Upper right: The MAP-CEM reconstruction Bottom left: The MAP-AEM reconstruction with the enhanced error model Bottom right: The MAP-AEM reconstruction with the complete error model.

shape of the cross section of the tank was obtained by segmenting a chest CT image. The measurement tank is vertically symmetric and the height of the tank is 5 cm. To construct the phantom, heart and lung shaped inclusions were made of agar and placed in the measurement tank filled with saline of conductivity $3.0\,\mathrm{mS\,cm}^{-1}$. The inclusions were constructed using vertically symmetric moulds. The conductivity of the lung and heart targets were 0.73 $\mathrm{mS\,cm}^{-1}$ and 5.8 $\mathrm{mS\,cm}^{-1}$, respectively.

4.4.2 Simultaneous estimation of the conductivity and approximation error

The samples of the approximation error due to unknown shape of the body were obtained similarly as in Section 4.3.1 using (4.7). The model domain $\tilde{\Omega}$ was a cylindrical domain with diameter ρ and the same samples $\gamma^{(\ell)}$ for the parameterization of the cross sections of sample domains $\Omega^{(\ell)}$ were used as in Section 4.3.1. The sample domains were vertically symmetric and the height of the sample domains were 5 cm (same as the height of the measurement domain). Thus no approximation errors due to truncation of the computation domain were present.

The estimation of the approximation error is conducted as follows. Let $\lambda_1 \geq \lambda_2 \geq \ldots \geq \lambda_m$ denote the eigenvalues of the covariance matrix Γ_ε and let $\{w_1, \ldots, w_m\}$ be the corresponding eigenbasis. Note that for the Gaussian approximation error

$$\varepsilon - \varepsilon_* \in \mathrm{sp}\{w_1, \ldots, w_m\}.$$

Using this relation, the realization of the modeling error is decomposed to mean plus two orthogonal components $(\varepsilon', \varepsilon'')$, that is

$$\varepsilon = \varepsilon_* + \underbrace{\sum_{k=1}^{p} \alpha_k w_k}_{\varepsilon'} + \underbrace{\sum_{j=p+1}^{m} \beta_j w_j}_{\varepsilon''}. \tag{4.11}$$

Using (4.11), the measurement model (2.15) is written in the modi-

fied form

$$V = U_\delta(\sigma, \tilde{\gamma}) + \sum_{k=1}^{p} \alpha_k w_k + \varepsilon_* + \varepsilon'' + e$$
$$= U_\delta(\sigma, \tilde{\gamma}) + W\alpha + \varepsilon_* + \varepsilon'' + e, \tag{4.12}$$

where $W = [w_1, w_2, \ldots, w_p]$ ($m \times p$ matrix), $\alpha = (\alpha_1, \alpha_2, \ldots, \alpha_p)^\mathrm{T} \in \mathbb{R}^p$, ε' represents a low-rank projection of ε in the basis of principal eigenvectors of Γ_ε, i.e. dimension p is chosen (significantly) smaller than m, and ε'' represents the non-estimated part of the approximation error. The dependence of the measurement model (4.12) on the boundary parametrization is embedded in the approximation error $\varepsilon = \varepsilon_* + W\alpha + \varepsilon''$.

Our objective is now to construct an approximation for the posterior density $\pi(\sigma, \alpha | V)$ using the measurement model (4.12) and estimate both the conductivity and the projection coefficients $\alpha \in \mathbb{R}^p$.

To obtain a computationally efficient approximation $\tilde{\pi}(\sigma, \alpha | V)$, we make the technical approximation that $(\sigma, \alpha, e, \varepsilon'')$ are mutually Gaussian and uncorrelated. Following the approach in [28], we obtain approximate likelihood

$$\tilde{\pi}(V | \sigma, \alpha) = \mathcal{N}(V - U_\delta(\sigma, \tilde{\gamma}) - W\alpha - \varepsilon_* - e_*, \Gamma_{\varepsilon''} + \Gamma_e)$$

and the approximate posterior density becomes

$$\tilde{\pi}(\sigma, \alpha \mid V) \propto \pi_+(\sigma)\tilde{\pi}(V | \sigma, \alpha)\pi(\sigma)\pi(\alpha). \tag{4.13}$$

By the properties of the eigenvalue decomposition, the prior distribution for the projection coefficients is $\pi(\alpha) = \mathcal{N}(0, \Gamma_\alpha)$, where $\Gamma_\alpha = \mathrm{diag}(\lambda_1, \lambda_2, \ldots, \lambda_p)$.

Comparing the present approach to the previous use of the approximation error approach (see e.g. [28, 97]), the main difference in the present approach is that the Gaussian approximation is pre-marginalized only partially over the approximation error and part of the approximation error is treated as unknown parameters.

The computation of the MAP estimate from the posterior model (4.13) amounts to solving the minimization problem

$$(\sigma, \alpha)_{\text{MAP}} = \arg \min_{\sigma \geq 0, \alpha} \left\{ || \, L_{\varepsilon'' + e}(V - U(\sigma, \tilde{\gamma}) - W\alpha - \varepsilon_* - e_*) \, ||^2 \right.$$

$$\left. + \, || \, L_{\sigma}(\sigma - \sigma_*) \, ||^2 + || \, L_{\alpha}\alpha \, ||^2 \right\}, \tag{4.14}$$

where the Cholesky factor $L_{\varepsilon'' + e}^{\mathrm{T}} L_{\varepsilon'' + e} = (\Gamma_{\varepsilon''} + \Gamma_e)^{-1}$, $L_{\alpha}^{\mathrm{T}} L_{\alpha} = \Gamma_{\alpha}^{-1}$ and $\Gamma_{\varepsilon''} = \sum_{p+1}^{m} \lambda_j w_j^{\mathrm{T}} w_j$.

4.4.3 Estimate for the boundary shape

Once the MAP estimation problem (4.14) has been solved, an approximate estimate for the boundary parameters γ of the actual domain Ω are estimated. For this, we use the Gaussian approximation of the joint density of $\varepsilon' = W\alpha$ and γ and find the MAP estimate

$$\gamma_{\text{MAP}} = \arg \max \tilde{\pi}(\gamma | \hat{\varepsilon}'), \tag{4.15}$$

given by

$$\hat{\gamma} = \Gamma_{\gamma \varepsilon'} \Gamma_{\varepsilon'}^{-1} \hat{\varepsilon}' + \gamma_*, \tag{4.16}$$

where $\hat{\varepsilon}' = W\alpha_{\text{MAP}}$ and γ_* is the prior mean of the boundary parameters. Furthermore, the posterior covariance is obtained as

$$\Gamma_{\hat{\gamma} | \hat{\varepsilon}'} = \Gamma_{\gamma} - \Gamma_{\gamma \varepsilon'} \Gamma_{\varepsilon'}^{-1} \Gamma_{\gamma \varepsilon'}^{\mathrm{T}}. \tag{4.17}$$

Note that the covariances $\Gamma_{\gamma \varepsilon'}$ and $\Gamma_{\varepsilon'}$ need to be estimated based on the Monte Carlo simulations. As previously said, the samples of the approximation error $\varepsilon^{(\ell)}$ were obtained using (4.7). In order to compute covariance matrices $\Gamma_{\gamma \varepsilon'}$ and $\Gamma_{\varepsilon'}$, the samples of the low-rank representation of the approximation error were obtained as

$$\varepsilon'^{(\ell)} = WW^{\mathrm{T}}(\varepsilon^{(\ell)} - \varepsilon_*). \tag{4.18}$$

Note that if there would be also other sources of approximation error than the unknown shape of the body (for example, discretization), then approximation errors in the measurement model should be separated. The separation of two approximation errors is represented in Section 4.1.2. By using the separation of approximation

errors, the basis vectors for the approximation errors due to pure domain modeling errors could be then computed and the approximation error could be estimated. Furthermore, the joint distribution of the pure approximation error due to body shape and the parameterization of the body shape could be constructed.

4.4.4 Representation of the conductivity in the estimated domain

The estimation (4.14) of the conductivity σ and the projection coefficients α is carried out in the model domain $\tilde{\Omega}$. Once the MAP estimates of σ, α and $\hat{\gamma}$ have been computed, the estimated conductivity σ is mapped from the model domain $\tilde{\Omega}$ into the reconstructed domain $\hat{\Omega}$ (that corresponds to parametrization $\hat{\gamma}$) by a linear interpolation

$$\hat{\sigma}_{\text{MAP}} = \tilde{P}\sigma_{\text{MAP}}, \tag{4.19}$$

where $\tilde{P}$ implements interpolation from domain to another according to the inverse T^{-1} of the domain deformation model (4.8).

4.4.5 Results

The MAP-CEM reconstruction using the correct measurement domain Ω (forward model $U_\delta(\sigma, \gamma)$) is shown in upper right Figure 4.4. This reconstruction can be taken as a reference estimate, since no approximation errors due to domain modeling are present. The MAP-CEM estimate computed using a cylindrical model domain (forward model $U_\delta(\sigma, \tilde{\gamma})$) is shown in middle left Figure 4.4. The reconstruction show intolerable reconstruction errors. The MAP-AEM reconstruction (forward model $U_\delta(\sigma, \tilde{\gamma}) + W\alpha$) is shown in middle right Figure 4.4. Note that this reconstruction is computed using the cylindrical model domain $\tilde{\Omega}$, however, the reconstruction is mapped to the estimated domain corresponding to estimated parameter $\hat{\gamma}$ using (4.19). The cross section of the actual domain Ω is shown as gray patch in bottom Figure 4.4. The reconstructed boundary corresponding to estimated parameter $\hat{\gamma}$ is shown with

solid line and 2 (*a posteriori*) standard deviation limits with dashed lines, for details of computation of 2 standard deviation limits, see Publication IV. As can be seen, the MAP-AEM reconstruction is significantly better than the MAP-CEM estimate and the estimated boundary shape is also feasible. Furthermore, the confidence limits of the estimated boundary are also feasible. In particular, the actual shape of the body is between the estimated 2 standard deviation limits. It was also found that infeasible estimates are obtained if the actual measurement domain has small probability with respect the prior model $\pi(\gamma)$, see Publication IV.
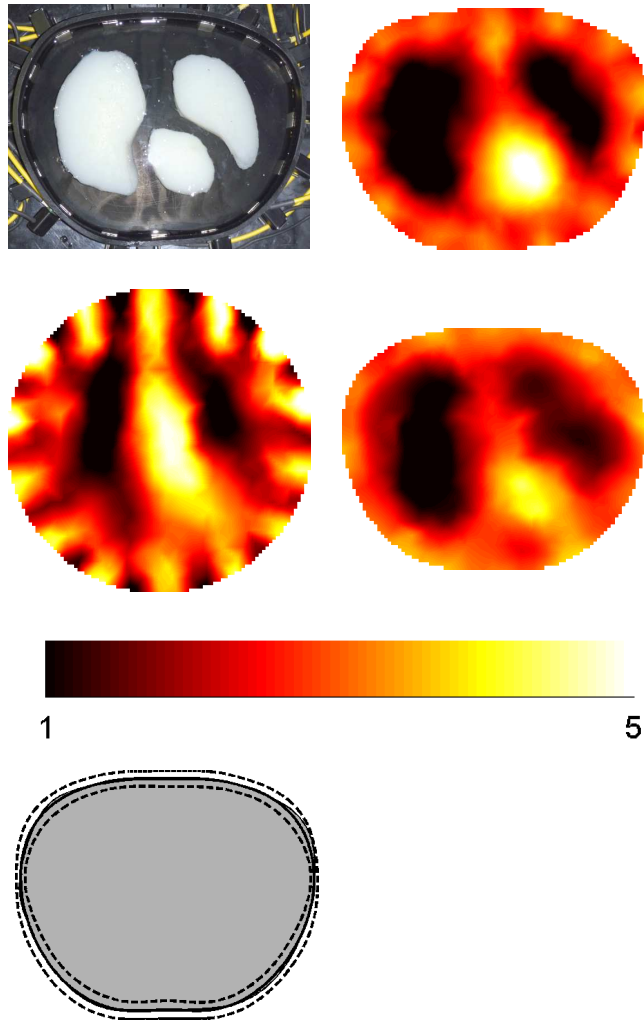
Figure 4.4: Top left: The measurement phantom. Top right: The MAP-CEM estimate computed using the correct computation domain. Middle left: MAP-CEM computed using the model domain. Middle right: MAP-AEM computed using the model domain and mapped to the estimated domain corresponding to estimated boundary parameters $\hat{\gamma}$. Bottom: The cross section of the actual domain Ω is shown as gray patch. The reconstructed boundary is shown with solid line and 2 (a posteriori) standard deviation limits with dashed lines.

5 Summary and conclusions

In this thesis, the approximation error approach was applied for errors due to reduced discretization, unknown boundary of the body, unknown contact impedances, and truncation of the computation domain. Furthermore, the approximation error approach was written in a novel way enabling the reconstruction of the conductivity and shape of the target body.

The motivation of the research stems from the practical applications of EIT in which reduced forward models have to be often used or the forward model contains unknown nuisance parameters. The reduced forward models are used typically due to limited computational resources and time. For example, in process tomography the reconstructions have to be typically computed within a few milliseconds. Typical examples of the unknown nuisance parameters in EIT are the unknown contact impedances and unknown parameterization of the shape of the body.

In Publication I, the errors due to reduced discretization and errors due to partially unknown geometry were compensated for by employing the approximation error approach. The approach was verified with real measurements from a measurement tank. It was found that the approximation error approach is useful in process monitoring applications in which the reconstructions should be computed in limited time and when the height of the surface of the liquid in a process vessel is unknown. The main advantage of the approximation error approach is that the the actual height of the liquid does not have to be known. Approximative knowledge of the height of the liquid is only required when the statistics of the approximation error is estimated.

In Publication II, the approximation error approach was applied for the errors due to unknown contact impedances, truncation of the computation domain and reduced discretization. The results were evaluated with laboratory measurements and also measure-

ments conducted in a pilot scale factory. The results indicate that these modeling errors can be compensated for efficiently. The solution of the inverse problem with the approximation error approach is less complicated with less tuning (prior parameters) since the contact impedances do not have to be estimated. Furthermore, the computation time with the approximation error approach is only fraction of that required with the conventional noise model.

In publication III, the errors due to reduced discretization and unknown shape of the body were compensated for by employing the approximation error approach. The computed examples concerned the chest imaging application when the reconstructions are computed using an approximate model domain. The approach was evaluated with both simulated and phantom measurements. It was found that both approximation errors can be compensated efficiently for by using the approximation error approach. In this study, the height of the model domain and actual domain were equal, i.e. truncation errors were not present in the measurements. However, this is not the case in clinical applications and the truncation of the computation domain should be modeled if the approach is applied for clinical measurements. Furthermore, in reality the cross section of the chest varies also with respect the vertical axis. In this study, the samples of the actual computation domains were obtained by segmenting 2D chest CT images. With clinical applications an atlas of 3D images might have to be used.

In Publication IV, the approximation error approach was written in a form enabling simultaneous reconstruction of conductivity and shape of the body. The boundary estimates and confidence limits of the estimates were feasible, i.e. the actual boundary was essentially between the estimated posterior uncertainty limits. An interesting further study would be to compute the reconstruction of the conductivity in two stages. First, estimate the conductivity and the shape of the computation domain and then estimate the conductivity using the estimated computation domain. This modified approach could be applied also for other unknown parameters such as unknown contact impedances. The simultaneous estimation of

the nuisance parameters with the approximation error approach could be also used with other inverse problems.

In many practical applications the absolute reconstructions are rarely computed since the computation burden with accurate models is prohibitively large. Furthermore, the construction of the accurate model requires accurate values of the nuisance parameters or these parameters have to estimated simultaneously with the conductivity leading to more complicated inverse problem with more prior parameters. In the approximation error approach, the accurate forward model is used only prior to the measurements when the statistics of the approximation error is estimated. Furthermore, the accurate values of the nuisance parameters are not needed; only the prior model of the nuisance parameters is used in the estimation of the approximation error statistics. In conclusions, feasible estimates can be computed efficiently with the reduced forward model in the inverse problem by employing the approximation error approach. Thus, it seems possible that the absolute EIT imaging could be used in applications that have been difficult so far with conventional noise models.

Bibliography

[1] M. Cheney, D. Isaacson, and J. C. Newell, "Electrical impedance tomography," *SIAM Rev* **41,** 85–101 (1999).

[2] J. P. Kaipio, V. Kolehmainen, E. Somersalo, and M. Vauhkonen, "Statistical inversion and Monte Carlo sampling methods in electrical impedance tomography," *Inv. Probl.* **16,** 1487–1522 (2000).

[3] L. Borcea, "Electrical impedance tomography," *Inv. Probl.* **18,** R99–R136 (2002).

[4] B. H. Brown, "Electrical impedance tomography (EIT): a review," *Journal of Medical Engineering and Technology* **27,** 97–108 (2003).

[5] R. Bayford, "Bioimpedance tomography (electrical impedance tomography)," *Annu Rev. Biomed. Eng.* **8,** 63–91 (2006).

[6] J. L. Mueller, D. Isaacson, and J. C. Newell, "Reconstruction of conductivity changes due to ventilation and perfusion from EIT data collected on a rectangular electrode array," *Physiol. Meas.* **22,** 97–106 (2001).

[7] J. Victorino, J. B. Borges, V. N. Okamoto, G. F. J. Matos, M. R. Tucci, M. P. R. Caramez, H. Tanaka, F. S. Sipmann, D. C. B. Santos, C. S. V. Barbas, C. R. R. Carvalho, and M. B. P. Amato, "Imbalances in regional lung ventilation," *Am. J. Respir. Crit. Care. Med.* **169,** 791–800 (2004).

[8] R. Bayford, P. Kantartzis, A. Tizzard, R. Yerworth, P. Liatsis, and A. Demosthenous, "Development of a neonate lung reconstruction algorithm using a wavelet AMG and estimated boundary form," *Physiol. Meas.* **29,** S125–S138 (2008).

[9] I. Frerichs, "Electrical impedance tomography (EIT) in applications related to lung and ventilation: a review of experimental and clinical activities," *Physiol. Meas.* **21,** R1–R21 (2000).

[10] T.-J. Kao, D. Isaacson, J. C. Newell, and G. J. Saulnier, "A 3D reconstruction algorithm for EIT using a handheld probe for breast cancer detection," *Physiol. Meas.* **27,** S1–S11 (2006).

[11] Y. Zou and Z. Guo, "A review of electrical impedance techniques for breast cancer detection," *Med. Eng. Phys.* **25,** 79–90 (2003).

[12] A. T. Tidswell, A. Gibson, R. H. Bayford, and D. S. Holder, "Validation of a 3D reconstruction algorithm for EIT of human brain function in a realistic head-shaped tank," *Physiol. Meas.* **22,** 117–185 (2001).

[13] O. C. Jones, J. T. Lin, , and L. Ovacik, "Investigation of electrical impedance imaging relative to two-phase, gas-liquid flows," *Chem. Eng. Comm.* **118,** 299–325 (1992).

[14] S. L. Ceccio and D. L. George, "Review of electrical impedance techniques for the measurement of multiphase flows," *J. Fluids Eng.* **118,** 391–399 (1996).

[15] F. J. Dickin, R. A. Williams, and M. S. Beck, "Determination of composition and motion of multicomponent mixtures in process vessels using electrical impedance tomography -I. principles and process engineering applications," *Chem. Eng. Sci.* **48,** 1883–1897 (1993).

[16] L. M. Heikkinen, J. Kourunen, T. Savolainen, P. J. Vauhkonen, J. P. Kaipio, and M. Vauhkonen, "Real time three-dimensional electrical impedance tomography applied in multiphase flow imaging," *Meas. Sci. Technol.* **17,** 2083 (2006).

[17] R. A. Williams and M. S. Beck, *Tomography: Principles, Techniques and Applications* (Butterworth-Heinemann, 1995).

[18] A. R. Ruuskanen, A. Seppänen, S. Duncan, E. Somersalo, and J. P. Kaipio, "Using process tomography as a sensor for optimal control," *Applied Numerical Mathematics* **56,** 37–54 (2006).

[19] R. A. Williams, X. Jia, and S. L. McKee, "Development of slurry mixing models using resistance tomography," *Powder technology* **87,** 21–27 (1996).

[20] M. A. Bennett and R. A. Williams, "Monitoring the operation of an oil/water separator using impedance tomography," *Minerals Eng* **17,** 605–614 (2004).

[21] A. Ramirez, W. Daily, A. Binley, D. LaBrecque, and D. Roelant, "Detection of leaks in underground storage tanks using electrical resistance methods," *J. Environ. Engng. Geophys.* **1,** 189–203 (1996).

[22] W. D. Daily and A. L. Ramirez, "Electrical imaging of engineering hydraulic barriers," *Geophysics* **65,** 83–94 (2000).

[23] W. D. Daily, A. L. Ramirez, D. J. LaBrecque, and J. Nitao, "Electrical resistivity tomography of vadose water movement," *Water Resour. Res.* **28,** 1429–1442 (1992).

[24] K. Karhunen, A. Seppänen, A. Lehikoinen, P. J. M. Monteiro, and J. P. Kaipio, "Electrical resistance tomography imaging of concrete," *Cement and Concrete Research* **40,** 137–145 (2010).

[25] D. Watzenig and C. Fox, "A review of statistical modeling and inference for electrical capacitance tomography," *Meas. Sci. Technol.* **20,** 052002 (2009).

[26] J. P. Kaipio and E. Somersalo, *Statistical and computational inverse problems* (Applied Mathematical Sciences 160, Springer-Verlag, 2005).

[27] J. P. Kaipio and E. Somersalo, "Statistical inverse problems: Discretization, model reduction and inverse crimes," *J. Comput. Appl. Math.* **198,** 493–504 (2007).

[28] V. Kolehmainen, T. Tarvainen, S. R. Arridge, and J. P. Kaipio, "Marginalization of uninteresting distributed parameters in inverse problems – Application to diffuse optical tomography," *Int. J. Uncertainty Quantification* **1,** 1–17 (2011).

[29] A. Lehikoinen, S. Finsterle, A. Voutilainen, L. M. Heikkinen, M. Vauhkonen, and J. P. Kaipio, "Approximation Errors and Truncation of Computational Domains with Application to Geophysical Tomography," *Inverse probl. Imaging* **1,** 371–389 (2007).

[30] S. Pursiainen, "Two-stage reconstruction of a circular anomaly in electrical impedance tomography," *Inv. Probl.* **22,** 1689–1703 (2006).

[31] S. R. Arridge, J. P. Kaipio, V. Kolehmainen, M. Schweiger, E. Somersalo, T. Tarvainen, and M. Vauhkonen, "Approximation errors and model reduction with an application in optical diffusion tomography," *Inv. Probl.* **22,** 175–195 (2006).

[32] V. Kolehmainen, M. Schweiger, I. Nissilä, T. Tarvainen, S. R. Arridge, and J. P. Kaipio, "Approximation errors and model reduction in three-dimensional diffuse optical tomography," *J. Opt. Soc. Am.* **26(10),** 2257–2268 (2009).

[33] J. Heino and E. Somersalo, "A modeling error approach for the estimation of optical absorption in the presence of anisotropies," *Phys. Med. Biol.* **49,** 4785–4798 (2004).

[34] J. Heino, E. Somersalo, and J. P. Kaipio, "Compensation for geometric mismodelling by anisotropies in optical tomography," *Opt. Express* **13,** 296–308 (2005).

[35] T. Tarvainen, V. Kolehmainen, A. Pulkkinen, M. Vauhkonen, M. Schweiger, S. R. Arridge, and J. P. Kaipio, "Approximation error approach for compensating modelling errors between the radiative transfer equation and the diffusion approximation in diffuse optical tomography," *Inv. Probl.* **26,** 015005 (18pp) (2010).

[36] D. Calvetti and E. Somersalo, *An Introduction to Bayesian Scientific Computing - Ten Lectures on Subjective Computing* (Springer, 2007), ISBN 978-0-387-73393-7.

[37] A. Tarantola, *Inverse Problem Theory and Methods for Model Parameter Estimation* (SIAM, Philadelphia, 2004).

[38] W. Gilks, S. Richardson, and D. Spiegelhalter, *Markov chain Monte Carlo in practice* (Chapman and Hall, London, 1996).

[39] C. Fox and G. Nicholls, "Sampling conductivity images via MCMC," in *The art and science of Bayesian image analysis* (1997), pp. 91–100.

[40] A. Christen and C. Fox., "MCMC using an approximation," *Journal of Computational and Graphical Statistics* **14,** 795–810, (2005).

[41] J. Nocedal and S. J. Wright, *Numerical Optimization (second edition)* (Springer, New York, 2006).

[42] K. J. Bathe, *Finite element procedures* (Prentice Hall, 1996).

[43] F. S. Moura, J. C. C. Aya, A. T. Fleury, M. B. P. Amato, and R. G. Lima, "Dynamic imaging in electrical impedance tomography of the human chest with online transition matrix identification," *IEEE Trans. Biomed. Im.* **57,** 422–431 (2010).

[44] T. Tarvainen, V. Kolehmainen, J. P. Kaipio, and S. R. Arridge, "Corrections to linear methods for diffuse optical tomography using approximation error modeling," *Biomedical Opt. Express* **1,** 209–222 (2010).

[45] J. M. J. Huttunen and J. P. Kaipio, "Approximation errors in nonstationary inverse problems," *Inverse Problems and Imaging* **1,** 77–93 (2007).

[46] J. M. J. Huttunen and J. P. Kaipio, "Approximation error analysis in nonlinear state estimation with an application to state-space identification," *Inv. Probl.* **23,** 2141–2157 (2007).

[47] J. M. J. Huttunen and H. K. Pikkarainen, "Discretization error in dynamical inverse problems: one-dimensional model case," *Journal of Inverse and Ill-posed problems* **15,** 365–386 (2007).

[48] J. M. J. Huttunen and J. P. Kaipio, "Model reduction in state identification problems with an application to determination of thermal parameters," *Appl. Num. Math.* **59,** 877–890 (2009).

[49] J. M. J. Huttunen, A. Lehikoinen, J. Hämäläinen, and J. P. Kaipio, "Importance filtering approach for the nonstationary approximation error method," *Inv. Probl.* **26,** 125003 (2010).

[50] A. Voutilainen and J. P. Kaipio, "Model reduction and pollution source identification from remote sensing data," *Inv. Probl. Imag.* **2,** 711–730 (2009).

[51] A. Lehikoinen, J. M. J. Huttunen, A. Voutilainen, S. Finsterle, M. Kowalsky, and J. P. Kaipio, "Dynamic inversion for hydrological process monitoring with electrical resistance tomography under model uncertainties," *Water resources research* **46,** W04513 (2010).

[52] A. Lipponen, A. Seppänen, and J. P. Kaipio, "Nonstationary inversion of convection-diffusion problems-recovery from unknown nonstationary velocity fields," *Inv. Probl. Imag.* **4,** 463–483 (2010).

[53] A. Lipponen, A. Seppänen, and J. P. Kaipio, "Reduced-order estimation of nonstationary flows with electrical impedance tomography," *Inv. Probl.* **26,** 074010 (2010).

[54] A. Lipponen, A. Seppänen, and J. P. Kaipio, "Nonstationary approximation error approach to imaging of three-dimensional pipe flow: experimental evaluation," *Meas. Sci. Technol.* **in review** (2011).

[55] K.-S. Cheng, D. Isaacson, J. C. Newell, and D. G. Gisser, "Electrode models for electric current computed tomography," *IEEE Trans. Biomed. Eng.* **36,** 918–924 (1989).

[56] E. Somersalo, M. Cheney, and D. Isaacson, "Existence and uniqueness for electrode models for electric current computed tomography," *SIAM J. Appl. Math.* **52,** 1023–1040 (1992).

[57] M. Vauhkonen, *Electrical impedance tomography and prior information*, PhD thesis (University of Kuopio, Finland, 1997).

[58] P. Vauhkonen, *Image reconstruction in three-dimensional electrical impedance tomography*, PhD thesis (University of Kuopio, 2004).

[59] L. M. Heikkinen, *Statistical estimation methods for electrical process tomography*, PhD thesis (University of Kuopio, Finland, 2005).

[60] P. J. Vauhkonen, M. Vauhkonen, T. Savolainen, and J. P. Kaipio, "Three-dimensional electrical impedance tomography based on the complete electrode model," *IEEE Trans. Biomed. Eng.* **46,** 1150–1160 (1999).

[61] V. Kolehmainen, *Novel approaches to image reconstruction in diffusion tomography*, PhD thesis (University of Kuopio, Finland, 2001).

[62] A. Seppänen, *State estimation in process tomography*, PhD thesis (University of Kuopio, 2005).

[63] A. P. Calderon, "On an inverse boundary value problem," in *Seminar on Numerical Analysis and its Applications to Continuum Physics* (1980), pp. 65–73.

[64] J. Sylvester and G. Uhlmann, "A global uniqueness theorem for an inverse boundary value problem," *Ann. of Math.* **125,** 153–169 (1987).

[65] A. I. Nachman, "Global uniqueness for a two-dimensional inverse boundary value problem," *Ann. Math.* **143,** 71–96 (1996).

[66] K. Astala and L. Päivärinta, "Caldern's inverse conductivity problem in the plane," *Ann. of Math.* **163,** 265–299 (2006).

[67] M. Vauhkonen, P. Karjalainen, and J. Kaipio, "A Kalman Filter Approach to Track Fast Impedance Changes in Electrical Impedance Tomography," *IEEE Trans. Biomed. Eng.* **45,** 486–493 (1998).

[68] A. Seppänen, M. Vauhkonen, P. J. Vauhkonen, E. Somersalo, and J. P. Kaipio, "State estimation with fluid dynamical evolution models in process tomography—an application to impedance tomography," *Inv. Probl.* **17,** 467–483 (2001).

[69] A. Seppänen, M. Vauhkonen, P. J. Vauhkonen, A. Voutilainen, and J. P. Kaipio, "State estimation in process tomography—three dimensional impedance imaging of moving fluids," *Int. J. Numer. Mthods Eng.* **73,** 1651–1670 (2008).

[70] P. Hua, J. Webster, and W. Tompkins, "A regularised electrical impedance tomography reconstruction algorithm," *Clin. Phys. Physiol. Meas.* **9,** 137–141 (1988).

[71] E. J. Woo, P. Hua, J. G. Webster, and W. J. Tompkins, "A robust image reconstruction algorithm and its parallel implementation in electrical impedance tomography," *IEEE Trans. Med. Im.* **12,** 137–146 (1993).

[72] B. H. Blott, G. J. Daniell, and S. Meeson, "Nonlinear reconstruction constrained by image properties in electrical impedance tomography," *Phys. Med. Biol* **43,** 1215–1224 (1998).

[73] M. Vauhkonen, D. Vadasz, P. Karjalainen, E. Somersalo, and J. Kaipio., "Tikhonov regularization and prior information in electrical impedance tomography," *IEEE Trans. Med. Imaging.* **17,** 285–293 (1998).

[74] M. Cheney, D. Isaacson, J. C. Newell, S. Simske, and J. Goble, "NOSER: An algorithm for solving the inverse conductivity problem," *Int. J. Imag. Systems and Technology* **2,** 66–75 (1990).

[75] D. C. Barber and B. H. Brown, "Applied potential tomography," *J. Phys. E: Sci. Instrum.* **17,** 723–733 (1984).

[76] F. Santosa and M. Vogelius, "A backprojection algorithm for electrical impedance imaging," *SIAM J. Appl. Math.* **50,** 216–243 (1990).

[77] C. J. Kotre, "A sensitivity coefficient method for the reconstruction of electrical impedance tomograms," *Clin Phys Physiol Meas, Suppl A* **10,** 275–281 (1989).

[78] J. Kourunen, R. Käyhkö, J. Matula, J. Käyhkö, M. Vauhkonen, and L. M. Heikkinen, "Imaging of two miscible liquids using electrical impedance tomography and linear impedance sensor," *Flow Measurement and Instrumentation* **19,** 391–396 (2008).

[79] E. L. V. Costa, C. N. Chaves, S. Gomes, M. A. Beraldo, M. S. Volpe, M. R. Tucci, I. A. L. Schettino, S. H. Bohm, C. R. R. Carvalho, H. Tanaka, R. G. Lima, and M. B. A. Amato, "Real-time detection of pneumothorax using electrical impedance tomography," *Crit. Care. Med.* **36,** 1230–1238 (2008).

[80] O. P. Tossavainen, M. Vauhkonen, L. M. Heikkinen, and T. Savolainen, "Estimating shapes and free surfaces with electrical impedance tomography," *Meas. Sci. Technol.* **15,** 1402–1411 (2004).

[81] O. P. Tossavainen, V. Kolehmainen, and M. Vauhkonen, "Free-surface and admittivity estimation in electrical impedance tomography," *Int. J. Num. Meth. Eng.* **66,** 1991–2013 (2006).

[82] P. J. Vauhkonen, M. Vauhkonen, and J. P. Kaipio, "Errors due to the truncation of the computational domain in static three-dimensional electrical impedance tomography," *Physiol. Meas.* **21,** 125–135 (2000).

[83] T. Vilhunen, J. P. Kaipio, P. J. Vauhkonen, T. Savolainen, and M. Vauhkonen, "Simultaneous reconstruction of electrode contact impedances and internal electrical properties: I. Theory," *Meas. Sci. Technol.* **13,** 1848–1854 (2002).

[84] L. M. Heikkinen, T. Vilhunen, R. M. West, and M. Vauhkonen, "Simultaneous reconstruction of electrode contact impedances and internal electrical properties: II. Laboratory experiments," *Meas. Sci. Technol.* **13,** 1855–1861 (2002).

[85] V. Kolehmainen, M. Vauhkonen, P. A. Karjalainen, and J. P. Kaipio, "Assessment of errors in static electrical impedance tomography with adjacent and trigonometric current patterns," *Physiol. Meas.* **18,** 289–303 (1997).

[86] V. Kolehmainen, M. Lassas, and P. Ola, "Electrical impedance tomography problem with inaccurately known boundary and contact impedances," *IEEE Trans. Med. Im.* **27,** 1404–1414 (2008).

[87] E. Gersing, B. Hoffmann, and M. Osypka, "Influence of changing peripheral geometry on electrical impedance tomography measurements," *Med. Biol. Eng. Comput.* **34,** 359–361 (1996).

[88] H. Jain, D. Isaacson, P. M. Edic, and J. C. Newell, "Electrical impedance tomography of complex conductivity distributions with noncircular boundary," *IEEE Trans. Biomed. Eng.* **44,** 1051–1060 (1997).

[89] J. Zhang and R. P. Pattersson, "EIT images of ventilation: what contributes to the resistivity changes?," *Physiol. Meas.* **26,** S81–S92 (2005).

[90] V. Kolehmainen, M. Lassas, and P. Ola, "The inverse conductivity problem with an imperfectly known boundary," *SIAM J. Appl. Math.* **66,** 365–383 (2005).

[91] V. Kolehmainen, M. Lassas, and P. Ola, "The inverse conductivity problem with an imperfectly known boundary in three dimensions," *SIAM J. Appl. Math.* **67,** 1440–1452 (2007).

[92] T. Dai, C. Gomez-Laberge, and A. Adler, "Reconstruction of conductivity changes and electrode movements based on EIT temporal sequences," *Physiol. Meas.* **29,** S77–S88 (2008).

[93] M. Soleimani, C. Comez-Laberge, and A. Adler, "Imaging of conductivity changes and electrode movement in EIT," *Physiol. Meas.* **27,** S103–S113 (2006).

[94] S. Siltanen, J. L. Mueller, and D. Isaacson, "An implementation of the reconstruction algorithm of A. Nachman for the 2-D inverse conductivity problem," *Inv. Probl.* **16,** 681–699 (2000).

[95] E. K. Murphy and J. L. Mueller, "Effect of domain shape modeling and measurement errors on the 2-D D-bar method for EIT," *IEEE Trans. Med. Im.* **28,** 1576–1584 (2009).

[96] A. Goshtasby, *2-D and 3-D Image Registration for Medical, Remote Sensing, and Industrial Applications* (Wiley Press, 2005).

[97] A. Nissinen, V. Kolehmainen, and J. P. Kaipio, "Compensation of modelling errors due to unknown domain boundary in electrical impedance tomography.," *IEEE Trans. Med. Im.* **30,** 231–242 (2011).

Antti Nissinen

Modelling Errors in Electrical Impedance Tomography

Recently, the Bayesian approximation error approach for the treatment of the approximation and modelling errors in inverse problems has been proposed. The key idea in the approximation error approach is to represent not only the measurement error, but also the effects of the computation model errors and uncertainties as an auxiliary additive noise process. In this thesis, the approach is applied in electrical impedance tomography (EIT) to compensate modeling errors due to reduced discretization, model reduction, unknown contact impedances and unknown shape of the body. The approach is evaluated with simulated and experimental data.

UNIVERSITY OF
EASTERN FINLAND